J. Fluid Mech. (2006), *vol.* 568, *pp.* 119–160.
doi:10.1017/S0022112006002631 Printed in the United Kingdom

Hydrodynamic interaction of two swimming model micro-organisms

By TAKUJI ISHIKAWA[1], M. P. SIMMONDS[2] AND T. J. PEDLEY[2]

[1]Department of Mechanical Engineering, University of Fukui, 3-9-1 Bunkyo, Fukui city 610-8507, Japan
ishikawa@pfsl.mech.tohoku.ac.jp

[2]Department of Applied Mathematics and Theoretical Physics, University of Cambridge, Centre for Mathematical Sciences, Wilberforce Road, Cambridge CB3 0WA, UK

(Received 4 March 2005 and in revised form 9 April 2006)

In order to understand the rheological and transport properties of a suspension of swimming micro-organisms, it is necessary to analyse the fluid-dynamical interaction of pairs of such swimming cells. In this paper, a swimming micro-organism is modelled as a squirming sphere with prescribed tangential surface velocity, referred to as a squirmer. The centre of mass of the sphere may be displaced from the geometric centre (bottom-heaviness). The effects of inertia and Brownian motion are neglected, because real micro-organisms swim at very low Reynolds numbers but are too large for Brownian effects to be important. The interaction of two squirmers is calculated analytically for the limits of small and large separations and is also calculated numerically using a boundary-element method. The analytical and the numerical results for the translational–rotational velocities and for the stresslet of two squirmers correspond very well. We sought to generate a database for an interacting pair of squirmers from which one can easily predict the motion of a collection of squirmers. The behaviour of two interacting squirmers is discussed phenomenologically, too. The results for the trajectories of two squirmers show that first the squirmers attract each other, then they change their orientation dramatically when they are in near contact and finally they separate from each other. The effect of bottom-heaviness is considerable. Restricting the trajectories to two dimensions is shown to give misleading results. Some movies of interacting squirmers are available with the online version of the paper.

1. Introduction

Massive plankton blooms are an integral part of the oceanic ecosystem. From the small night-time grazers that ascend from the (relatively safe) depths of the oceans to feast on phytoplankton, descending from the water surface at night to increase their nutrient uptake, to the largest animals on Earth, (plankton-grazing) blue whales, there is an essential dependence on populations of micro-organisms. Moreover, it is not only in the oceanic ecosystem that dense populations of micro-organisms have a considerable influence on human life. They are used in biotechnology, they sometimes cause harmful red tides in coastal regions of the ocean and they absorb CO_2, which affects the global climate.

The size of individual micro-organisms is often much smaller than that of the flow field of interest, especially in an oceanic plankton bloom. In such cases, the suspension is modelled as a continuum in which the variables are volume-averaged quantities

(Fasham, Ducklow & McKelvie 1990; Pedley & Kessler 1992; Metcalfe, Pedley & Thingstat 2004). Continuum models for suspensions of swimming micro-organisms have also been proposed for the analysis of phenomena such as bioconvection (Childress, Levandowsky & Spiegel 1975; Pedley & Kessler 1990; Hillesdon, Pedley & Kessler 1995; Bees & Hill 1998; Metcalfe & Pedley 2001, for instance). However, the continuum models proposed so far have been restricted to dilute suspensions, in which cell–cell interactions are negligible. If one wishes to consider larger cell concentrations, for example in the dense falling plumes that form part of bioconvection patterns (Kessler *et al.* 1994; Metcalfe & Pedley 2001), it will be necessary to consider interactions between micro-organisms. Then the translational–rotational velocities of the micro-organisms, the particle stress tensor and the diffusion tensor in the continuum model will need to be replaced by improved expressions.

To model the motion of a real micro-organism mathematically is a massive undertaking. Micro-organisms exist over a large range of length scales (roughly 1–500 μm for common marine species) and alter their behaviour depending on many parameters relating to their environment. The variety of shapes both inter- and intraspecies is also vast. Indeed, even individual micro-organisms do not maintain the same shape and often change to eat, reproduce or protect themselves from predators or hostile environments. Any model capable of being analysed mathematically will therefore need to make severe simplifications, even for the simplest micro-organisms (Brennen & Winet 1977). The model micro-organism used in this paper will, by necessity, be extremely primitive and many non-biological assumptions will be made. The model micro-organisms we have used are the simplest we could think of that both swim and have finite size, so that excluded-volume effects and hydrodynamic interactions can be analysed non-trivially.

First it will be assumed that such a micro-organism has a spherical shape. This assumption is made for obvious mathematical convenience, but a number of real micro-organisms, notably ciliates such as *Opalina* and colonies of flagellates such as *Volvox* (Brennen & Winet 1977; Larson, Kirk & Kirk 1992) are roughly spherical. Cyanobacteria (Waterbury *et al.* 1985) also have no external appendages, and the cell body is approximately a spheroid with aspect ratio about 2. They swim by a bulk streaming of the cell surface without observable shape change (Pitta & Berg 1995). The creatures will also be assumed to be neutrally buoyant, because the sedimentation velocity for typical aquatic micro-organisms is much less than the swimming speed. The centre of buoyancy of the spherical micro-organism may not coincide with its geometric centre. This provides the micro-organism with a self-righting mechanism, causing it to move in a preferred direction even if temporarily advected or rotated by the flow in another direction (Pedley & Kessler 1987). Certain swimming algae are bottom-heavy, for example, enabling them to swim vertically upwards (on average) in still water (Kessler 1986). The model micro-organism is, therefore, force free but may not be torque free. The swimming speeds of micro-organisms range up to several hundred μm s^{-1}. The Reynolds number based on the swimming speed and the radius of individuals is usually less than 10^{-2}, therefore the flow field around the micro-organisms is assumed to be Stokes flow. Brownian motion is not taken into account, because typically micro-organisms are too large for Brownian effects to be important although often they appear to reorientate randomly while swimming, in a manner which may be analogous to Brownian motion (Pedley & Kessler 1990; Hill & Häder 1997; Vladimirov *et al.* 2004).

The model micro-organism will be assumed to propel itself by generating tangential velocities on its surface. Again, this is the simplest model that is susceptible to

analysis. In fact, it is a reasonable model to describe the locomotion of certain ciliates, which propel themselves by beating arrays of short hairs (cilia) on their surface in a synchronized way. In particular, the so-called symplectic metachronal wave employed by *Opalina*, for instance, in which the cilia tips remain close together at all times, can be modelled simply as the stretching and displacement of the surface formed by the envelope of these tips, and this can be regarded as approximately spherical (Blake 1971; Brennen 1974). We make the additional simplification that the small radial displacement of this envelope can be neglected, and the boundary conditions applied on the sphere's surface. Furthermore, the tangential motions on the spherical surface will be assumed to be axisymmetric and time independent. The latter assumption is not justified for ciliates such as *Opalina*, which beat the cilia at a frequency of around 80 Hz, but if it is permissible to average over many beat cycles then the present model can be taken to refer to the mean motion. Details of this model micro-organism are given explicitly in Appendix A; it will be referred to as a *squirmer*. The velocity field generated by a squirmer is shown graphically in figure 1. The model of a squirmer was first proposed by Lighthill (1952), and his analysis was then extended by Blake (1971). The model was used by Magar, Goto & Pedley (2003) to analyse the nutrient-uptake properties of a solitary squirmer.

Much work has been done to analyse the effect of hydrodynamic interactions in a suspension of inert spheres in a Stokes-flow regime. This research field was pioneered by Batchelor (1970). Brady and his colleagues calculated the particle stress tensor and diffusion tensor for spheres in a simple shear flow and in a pressure-driven flow by using Stokesian-dynamics simulations (Brady & Bossis 1988; Nott & Brady 1994). This simulation method constructs a mobility matrix for the force, torque and stresslet based on precise expressions for two-sphere interactions, and the many-body interaction is taken into account by inverting the mobility matrix (because inverting the mobility matrix sums an infinite number of reflected interactions among particles, as discussed in Durlofsky, Brady & Bossis 1987). The stresslet is necessary in considering the stress field of a suspension and for improving the accuracy of a Stokesian-dynamics simulation. Therefore, a precise analysis of the force, torque and stresslet of two interacting spheres is the starting point for the many-body problem. Claeys & Brady (1989) analysed a suspension of inert spheroids under a simple shearing motion using a Stokesian-dynamics simulation, beginning with a two-spheroid interaction then using this to construct the mobility matrix for many-body interactions (Claeys & Brady 1993). Similarly, in order to analyse a non-dilute suspension of swimming micro-organisms, it is first necessary to obtain precise expressions for the force, torque and stresslet of two interacting micro-organisms. Then it may be extended to many bodies. The present paper is concerned with two-body interactions.

The electrophoretic motions of interacting charged particles have been widely investigated (Prieve *et al.* 1984; Ken & Anderson 1985; Baygents, Rivette & Stone 1998, for instance). In the dilute limit, the charged particles actually swim in the direction of the applied electric field. This characteristic as an *active* particle is somewhat analogous to bottom-heavy micro-organisms, which swim upwards. However, the electric charge is normally induced passively on the particle and there is no preferred direction associated with an individual sphere. This means that there is no overall torque on a charged sphere, which is different from the case of a bottom-heavy sphere in a gravitational field. Moreover, when two charged particles are in near contact, their electric fields change passively.

This characteristic is also different from the case of our squirmers, which are assumed to swim actively even when two of them are in near contact. Therefore, earlier research on electrophoretic motion cannot be simply extended to study the interaction of active micro-organisms.

There have been a few investigations of hydrodynamic interactions between micro-organisms previously. Guell *et al.* (1988) discussed the flow field far from a spherical body with a rotating helical flagellum (modelling a swimming bacterium). Ramia, Tullock & Phan-Thien (1993) and Nasseri & Phan-Thien (1997) also investigated the interaction between two spheroidal bodies with rotating helical flagella, by using a boundary-element method. Their computational conditions were limited to two cases, that of swimming side by side and that of swimming along one line. The minimum distance between the two spheroidal bodies was taken to be approximately equal to the minor axis of either spheroid, and they did not examine bodies in near contact. Recently, Lega & Passot (2003) derived a hydrodynamic model for bacterial colonies suspended on an agar plate. To model nutrient transfer and hydrodynamics, the authors had to include an *ad hoc* interactive force acting between the micro-organisms that in practice is unlikely to exist. Jiang, Osborne & Meneveau (2002) used a numerical hydrodynamic model for two swimming organisms (copepods, which are significantly larger than single-celled ciliates or flagellates) to calculate prey-encounter rates and other important quantities; they concluded that the behaviour of micro-organisms is very different when they are close together. However, the cse of two micro-organisms in near contact was not analysed mechanistically in any of these former studies.

It is to be expected that in the presence of a nearby micro-organism any given micro-organism will not behave as if it were alone. It may attempt to reproduce sexually or to consume (or avoid being consumed by) its neighbour. It may also move away from it to avoid competition for food. However, the hydrodynamic interaction of micro-organisms has not yet been modelled precisely and so considering only passive interactions (where the micro-organisms do not actively react to the presence of others) is a worthwhile approach in a first model. Throughout this paper the squirming motion of a sphere's surface is assumed to be invariant, except in § 6 where the condition of constant swimming power is applied as an alternative.

When two micro-organisms are far enough apart the hydrodynamic interaction between them is rather simple. In terms of a multipole expansion, the interaction can be described by using only the second moment, a force dipole. However, two micro-organisms in near contact are rather difficult to deal with. For rigid surfaces in relative motion, the flow in the gap region dominates and lubrication theory provides the leading term in an asymptotic expansion. For shearing motions (two surfaces sliding past each other) the leading term in the force–velocity correlation is $O(\log \varepsilon^{-1})$, where ε is the gap distance, and thus dominates the solution only in the mathematical sense. Even if we take ε as the ratio of molecular to macroscopic dimensions, $\log \varepsilon^{-1}$ is not large enough to dominate, and the next-order, $O(1)$, term must be included. The $O(1)$ term cannot be obtained by an asymptotic analysis of the region near the gap, because all regions of the particle surface contribute to it (Kim & Karrila 1992). Thus a numerical solution is unavoidable.

In § 2 of this paper, the far-field flow properties will be calculated analytically, by exploiting the Fáxen relations, and in § 3 the near-field flow properties will be calculated analytically using lubrication theory. The intermediate-field flow properties will be calculated numerically in § 4, using a boundary-element method, and then the analytical and numerical results will be compared. In these sections, the principal

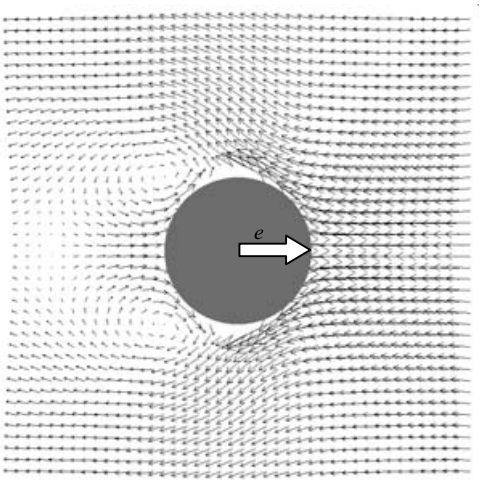

FIGURE 1. Flow velocity vectors relative to the translational velocity vector of a solitary squirmer with $\beta = 5$ in a uniform flow, of speed 1.0 in dimension-free form, coming from the far right.

derived quantities will be the translational–rotational velocities and the stresslet of an interacting pair of squirmers. The bulk stress of a suspension of squirmers can be expressed using the stresslet, as discussed in Batchelor (1970), which is why the stresslet of an interacting pair of squirmers needs to be calculated first. In a future paper, we intend to use the results of this paper to investigate the behaviour of suspensions of many squirmers, using the technique of Stokesian dynamics. It is therefore worthwhile generating a database for interacting pairs of squirmers from which arbitrary pairwise interactions can be looked up or interpolated. The stresslet is also necessary for improving the accuracy of the Stokesian-dynamics simulation. Details of the database will be explained in § 5.† The behaviour of two interacting squirmers is discussed phenomenologically and for results the trajectories of two squirmers are also given in § 5. Some movies of interacting squirmers are available with the online version of the papers. In § 6, we will summarize the results and discuss the effect of boundary conditions on the squirmer surface.

2. Analysis for far-field separation

The solutions for the flow and the stresslet generated by a solitary squirmer are given explicitly in Appendix A in dyadic notation; some symbols defined in Appendix A will be used here without repeating their definitions.

The velocity field generated by a solitary squirmer with $B_2/B_1 = 5$ ($B_n = 0$ for $n > 2$) is shown in figure 1. A solitary, force-free squirmer swims with speed $U = 2B_1/3$, from (A 7). (Stone & Samuel (1996) derived an analytical result for the swimming speed of a micro-organism propelled by surface distortions in terms of the surface velocities. However, in our case the surface velocity of a squirmer includes its swimming speed, so their method does not yield new information.) The far-field flow properties will be calculated by exploiting the Fáxen relations. The linearity of the problem means that the solution for two inert spheres in a background flow field can be added to the

† The database, which covers a wide range of parameters, is available from the first author

solution for two squirmers in a fluid otherwise at rest to calculate the general solution for two squirmers in a background flow field. The velocities and angular velocities of the squirmers (with the background flow) are then the sums of the solutions for squirmers in a still fluid and for inert spheres in a background straining flow. The construction of the solutions will follow a similar approach to that of established texts (e.g. Kim & Karrila 1992; Russel, Saville & Schowalter 1992).

2.1. *Velocity difference*

To express the velocity difference of the two squirmers in general terms, consider the velocity field generated by a squirmer centred at the origin, with radius a, squirming set $\boldsymbol{B}$ and orientation vector $\boldsymbol{e}$. Let this be $\mathscr{V}$, where, from (A 8),

$$\mathscr{V}(\boldsymbol{x}, a, \boldsymbol{e}, \boldsymbol{B}) = -\frac{1}{3}\frac{a^3}{r^3}B_1\boldsymbol{e} + B_1\frac{a^3}{r^3}\frac{\boldsymbol{e}\cdot\boldsymbol{r}}{r}\frac{\boldsymbol{r}}{r} + \sum_{n=2}^{\infty}\left(\frac{a^{n+2}}{r^{n+2}} - \frac{a^n}{r^n}\right)B_n P_n\left(\frac{\boldsymbol{e}\cdot\boldsymbol{r}}{r}\right)\frac{\boldsymbol{r}}{r} + \sum_{n=2}^{\infty}\left(\frac{n}{2}\frac{a^{n+2}}{r^{n+2}} - \left(\frac{n}{2}-1\right)\frac{a^n}{r^n}\right)B_n W_n\left(\frac{\boldsymbol{e}\cdot\boldsymbol{r}}{r}\right)\left(\frac{\boldsymbol{e}\cdot\boldsymbol{r}}{r}\frac{\boldsymbol{r}}{r} - \boldsymbol{e}\right). \quad (2.1)$$

Let the flow solution (A 8) for a solitary squirmer with centre at $\boldsymbol{x}_0$, radius a and squirming set $\boldsymbol{B}^{(1)}$ (i.e. the set of modes of the squirming motion, $B_1^{(1)}, B_2^{(1)}, \ldots$) be $\boldsymbol{u}_{sol}$ in the frame in which the fluid is at rest far away. Then if a new squirmer is added to this flow field at $\boldsymbol{x}_0 + \boldsymbol{r}$, with radius αa and squirming set $\boldsymbol{B}^{(2)}$, Fáxen's first law is given as (Russel *et al.* 1992)

$$\boldsymbol{F}_2 = 6\pi\mu\alpha a\left(\frac{2}{3}B_1^{(2)}\boldsymbol{e}_2 - \boldsymbol{U}_2 + \left(\boldsymbol{u}_{sol} + \frac{\alpha^2 a^2}{6}\nabla^2\boldsymbol{u}_{sol}\right)\Big|_{\boldsymbol{x}_0+\boldsymbol{r}}\right), \quad (2.2)$$

where $\boldsymbol{F}_2$ is the force exerted on the second squirmer, $\boldsymbol{e}_2$ is the orientation vector of the second squirmer and $\boldsymbol{U}_2$ is its velocity. Since the second squirmer moves with velocity $\frac{2}{3}B_1^{(2)}\boldsymbol{e}_2$ in the absence of the first squirmer, the first term on the right-hand side is added to Fáxen's first law for a inert sphere. By assuming a force-free squirmer, (2.2) can be transformed to

$$\boldsymbol{U}_2 = \frac{2}{3}B_1^{(2)}\boldsymbol{e}_2 + \left(\boldsymbol{u}_{sol} + \frac{\alpha^2 a^2}{6}\nabla^2\boldsymbol{u}_{sol}\right)\Big|_{\boldsymbol{x}_0+\boldsymbol{r}}. \quad (2.3)$$

Of course the original squirmer causes a perturbation to the velocity field of the second, but these higher-order terms are neglected here.

Defining the separation velocity as $\mathrm{d}\boldsymbol{U} = \boldsymbol{U}_2 - \boldsymbol{U}_1$ yields the following expression for $\mathrm{d}\boldsymbol{U}$:

$$\mathrm{d}\boldsymbol{U} = \frac{2}{3}B_1^{(2)}\boldsymbol{e}_2 - \frac{2}{3}B_1^{(1)}\boldsymbol{e}_1 + \mathscr{V}\left(\boldsymbol{r}, a, \boldsymbol{e}^{(1)}, \boldsymbol{B}^{(1)}\right) + \frac{\alpha^2 a^2}{6}\nabla^2\mathscr{V}\left(\boldsymbol{r}, a, \boldsymbol{e}^{(1)}, \boldsymbol{B}^{(1)}\right) - \mathscr{V}\left(-\boldsymbol{r}, \alpha a, \boldsymbol{e}^{(2)}, \boldsymbol{B}^{(2)}\right) - \frac{a^2}{6}\nabla^2\mathscr{V}\left(-\boldsymbol{r}, \alpha a, \boldsymbol{e}^{(2)}, \boldsymbol{B}^{(2)}\right). \quad (2.4)$$

2.2. *Rotational velocities*

The rotational velocity of the first squirmer in the same arrangement as in the previous section can be given by Fáxen's second law (Russel *et al.* 1992):

$$\boldsymbol{T}_1 = 8\pi\mu a^3\left(-\boldsymbol{\Omega}_1 + \tfrac{1}{2}\nabla\wedge\mathscr{V}\left(-\boldsymbol{r}, \alpha a, \boldsymbol{e}^{(2)}, \boldsymbol{B}^{(2)}\right)\right), \quad (2.5)$$

where $\boldsymbol{T}_1$ is the torque exerted on the first squirmer. If the squirmer is bottom heavy, there will be a torque acting on it and this must be equal and opposite to the

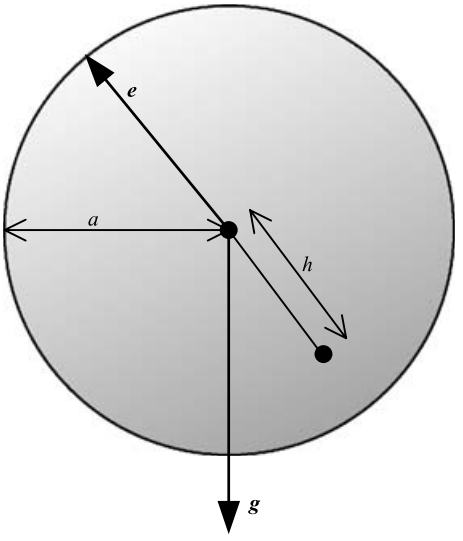

FIGURE 2. The arrangement of a bottom-heavy squirmer. Gravity acts in the $\boldsymbol{g}$-direction, and the squirmer has orientation vector $\boldsymbol{e}$, radius a and centre-of-mass distance h from its geometrical centre.

hydrodynamic torque, so that the net torque on the squirmer is zero. If the distance of the centre of gravity to the centre of the squirmer is h, in the opposite direction to its swimming direction in undisturbed fluid (see figure 2), then there is an additional torque equal to

$$\tfrac{4}{3}\pi a^3 \rho h \boldsymbol{e} \wedge \boldsymbol{g}, \tag{2.6}$$

where ρ is the density and $\boldsymbol{g}$ is the gravitational acceleration. This torque must be matched by the hydrodynamic torque, $\boldsymbol{T}$. Thus

$$\boldsymbol{\Omega}_1 = -\frac{\rho}{6\mu} h \boldsymbol{e}_1 \wedge \boldsymbol{g} + \nabla \wedge \mathscr{V}\big(-\boldsymbol{r}, \alpha a, \boldsymbol{e}^{(2)}, \boldsymbol{B}^{(2)}\big). \tag{2.7}$$

The correction to the rotational velocity due to the effect of the movement of the first sphere on the second sphere and the consequent effect back on the first sphere is of order

$$O\left(\left|\frac{B_2^{(1)}}{a}\right| \frac{a^6}{r^6} \boldsymbol{r} \wedge \boldsymbol{e}\right), \tag{2.8}$$

which is much smaller.

2.3. *Stresslets*

The stresslet of the first squirmer in the same arrangement as above is given by Fáxen's second law (Russel *et al.* 1992):

$$\boldsymbol{S}_1 = \frac{4\pi}{3}\mu a^2 (3\,\boldsymbol{e}_1\boldsymbol{e}_1 - \boldsymbol{I}) B_2^{(1)} + \frac{10}{3}\pi\mu a^3 \left(1 + \frac{a^2}{10}\nabla^2\right) \mathscr{E}\big(-\boldsymbol{r}, \alpha a, \boldsymbol{e}^{(2)}, \boldsymbol{B}^{(2)}\big). \tag{2.9}$$

The first term on the right-hand side is the stresslet of a solitary squirmer, given by equation (A 14); $\mathscr{E}$ is the rate of strain of a solitary squirmer, defined as $\mathscr{E} = \frac{1}{2}(\nabla\mathscr{V} + \nabla(\mathscr{V})^t)$, and can be calculated term by term. The first mode ($n = 1$),

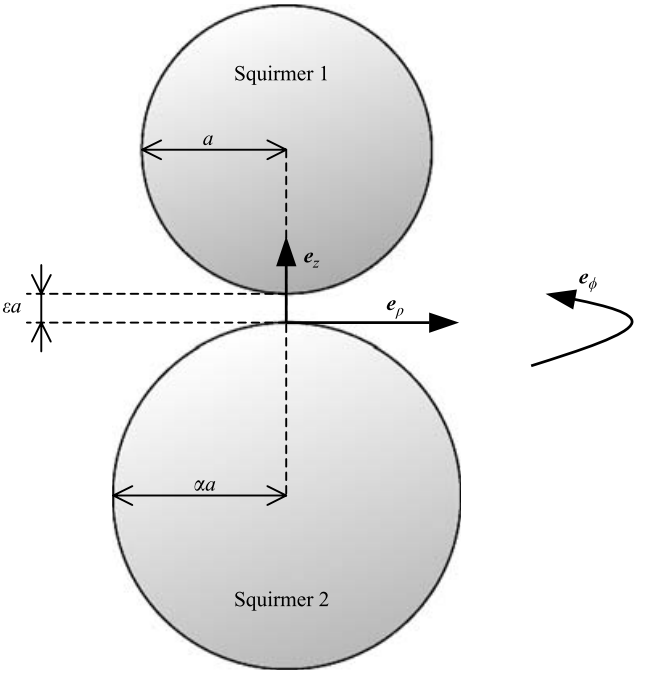

FIGURE 3. Diagram of the geometry for two near-separated squirmers. The vector $\boldsymbol{e}_z$ denotes the direction of squirmer 1 from squirmer 2, while $\boldsymbol{e}_\rho$ points radially out from that vector and $\boldsymbol{e}_\phi$ is azimuthal.

for example, gives the result

$$\mathscr{E}(\boldsymbol{r}, a, \boldsymbol{e}, \boldsymbol{B}) = \frac{a^3}{r^4}\left(\frac{\boldsymbol{e}\cdot\boldsymbol{r}}{r}\boldsymbol{I} - 5\frac{\boldsymbol{e}\cdot\boldsymbol{r}}{r}\frac{\boldsymbol{r}\boldsymbol{r}}{r^2} + \frac{\boldsymbol{e}\boldsymbol{r}+\boldsymbol{r}\boldsymbol{e}}{r}\right) B_1. \tag{2.10}$$

3. Analysis for near-field separation

The other regime of importance in $\boldsymbol{r}$-space is the *near field*, which can be defined as the region including values of r such that $r-(1+\alpha)a \ll (1+\alpha)a$. In this region one can use lubrication theory to calculate the velocities, angular velocities and stresslets of the two squirming spheres. As in the previous section, the problem is linear in the velocity field, and hence the problem of two squirming spheres in a fluid that is at rest at infinity can be solved and then added to the solution for two inert spheres in a linear background-flow field. The rigid-sphere case has been studied extensively, with contributions from Batchelor & Green (1972*a*), and a general outline of the method is included in standard texts (e.g. Kim & Karrila 1992).

Let the two spheres, 1 and 2 say, have radii a and αa, orientation vectors $\boldsymbol{e}_1$ and $\boldsymbol{e}_2$ and squirming sets $\boldsymbol{B}^{(1)}$ and $\boldsymbol{B}^{(2)}$, respectively. Let the z-axis pass through the two sphere centres and let $z=0$ be the plane containing the point on sphere 2 closest to sphere 1 (so that sphere 2 is in the region $z\leqslant 0$ and sphere 1 in $z>0$). Let the surfaces of the spheres be determined by $z=h_1$ and $z=h_2$ (for spheres 1 and 2 respectively). Furthermore let the minimum separation of the spheres be εa (with $\varepsilon \ll 1$) and assume that $\alpha = O(1)$ (i.e. the spheres are comparable in size). This is illustrated in figure 3.

To find the difference in velocity one can consider a frame in which sphere 2 is fixed and the centre of sphere 1 moves with velocity $\boldsymbol{V}-\boldsymbol{\Omega}'\wedge\boldsymbol{r}$, where $\boldsymbol{V}$ is the separation

velocity (i.e. the velocity of sphere 1 less the velocity of sphere 2), $\boldsymbol{\Omega}'$ is the angular velocity of sphere 2 and $\boldsymbol{r}$ is the separation vector between the two sphere centres ($\boldsymbol{r} = \boldsymbol{r}_1 - \boldsymbol{r}_2$).

The problem is governed by the Stokes equations,

$$\mu \nabla^2 \boldsymbol{u} = \nabla p, \quad \nabla \cdot \boldsymbol{u} = 0, \tag{3.1}$$

where the velocity of the fluid is $\boldsymbol{u}$, its viscosity is μ and p is the pressure. The boundaries of the two squirmers are defined by

$$h_1 = a\left(\varepsilon + \frac{\rho^{*2}}{2a^2} + O\left(\frac{\rho^{*4}}{a^4}\right)\right), \quad h_2 = -\alpha a\left(\frac{\rho^{*2}}{2\alpha^2 a^2} + O\left(\frac{\rho^{*4}}{a^4}\right)\right), \tag{3.2}$$

for squirmers 1 and 2 respectively; here $\rho^* = \sqrt{x^2 + y^2}$ and x and y are defined in Cartesian coordinates. To make the boundary conditions order 1, the following scaling is then used:

$$\varepsilon^{1/2} a X = x, \quad \varepsilon^{1/2} a Y = y \left(\Longrightarrow \varepsilon^{1/2} a \rho = \rho^*\right), \quad \varepsilon a Z = z. \tag{3.3}$$

This then defines the problem as follows:

$$\left(\varepsilon \nabla_\perp^2 + \frac{\partial^2}{\partial Z^2}\right) \boldsymbol{u} = \varepsilon \left(\varepsilon^{1/2} \frac{\partial p}{\partial X}, \varepsilon^{1/2} \frac{\partial p}{\partial Y}, \frac{\partial p}{\partial Z}\right), \quad \varepsilon^{1/2} \left(\frac{\partial u}{\partial X} + \frac{\partial v}{\partial Y}\right) + \frac{\partial w}{\partial Z} = 0, \tag{3.4}$$

$$H_1 = 1 + \frac{\rho^2}{2} + O(\varepsilon), \quad H_2 = -\frac{\rho^2}{2\alpha} + O(\varepsilon), \tag{3.5}$$

where $h_{1,2} = \varepsilon a H_{1,2}$ and

$$\nabla_\perp = \left(\frac{\partial}{\partial X}, \frac{\partial}{\partial Y}, 0\right) \tag{3.6}$$

is the dimensionless scaled gradient operator in the plane perpendicular to the line joining the centres. The velocities and pressure have not yet been scaled or non-dimensionalized; this will be done later in this section when a scale for velocity has been found (there are several velocity scales, such as $\boldsymbol{B}_i^{(1)}$ for any $i \geqslant 1$).

It is now possible to exploit the linearity of the Stokes equations to decompose this problem into two simpler problems. The first has the squirming-sphere boundary conditions on sphere 1 and zero velocity on sphere 2. The second problem is the complementary one, of zero velocity on sphere 1 and the squirming-sphere boundary conditions on sphere 2. Solving one of these problems will trivially provide a solution to the other, so without loss of generality we will consider the first problem. Thus the velocity on $Z = H_2(X, Y)$ is $\mathbf{0}$ and the velocity on sphere 1 (where $Z = H_1(X, Y)$) is

$$\sum_n \left[B^{(1)}\right]_n W_n \left(\frac{\boldsymbol{e}_1 \cdot \boldsymbol{r}_1}{r_1}\right) \left(\frac{\boldsymbol{e}_1 \cdot \boldsymbol{r}_1}{r_1} \frac{\boldsymbol{r}_1}{r_1} - \boldsymbol{e}_1\right) + \frac{2}{3}\left[B^{(1)}\right]_1 \boldsymbol{e}_1, \tag{3.7}$$

where

$$\boldsymbol{r}_1 = \boldsymbol{r} - (1 + \varepsilon) a \boldsymbol{e}_Z, \quad \boldsymbol{e}_Z = (0, 0, 1), \tag{3.8}$$

which defines unscaled coordinates of the same orientation as $\boldsymbol{r}$ but with their origin at the centre of sphere 1. Since the orientation and squirming set of sphere 2 are not present in this problem, without loss of generality we define $\boldsymbol{e} = \boldsymbol{e}_1$ and $\boldsymbol{B} = \boldsymbol{B}^{(1)}$. The constant velocity on the surface of sphere 1 (i.e. the last term in (3.7)) can be absorbed into the solid-body motion of one sphere (with another nearby sphere fixed in space). Hence the term $\frac{2}{3} B_1 \boldsymbol{e}$ in (3.7) can be neglected.

Expanding (3.7) in terms of $\varepsilon^{1/2}$ gives the velocity on sphere 1 as

$$\boldsymbol{u} = \boldsymbol{u}_0 + \varepsilon^{1/2}\boldsymbol{u}_1 + O(\varepsilon), \tag{3.9}$$

where $\boldsymbol{\rho} = (X, Y, 0)$ and

$$\boldsymbol{u}_0 = \sum_n B_n W_n(\boldsymbol{e}\cdot\boldsymbol{e}_z)\,(\boldsymbol{e}\cdot\boldsymbol{e}_z\,\boldsymbol{e}_z - \boldsymbol{e}), \tag{3.10}$$

$$\boldsymbol{u}_1 = \sum_n B_n W_n(\boldsymbol{e}\cdot\boldsymbol{e}_z)(\boldsymbol{e}\cdot\boldsymbol{\rho}\,\boldsymbol{e}_z + \boldsymbol{e}\cdot\boldsymbol{e}_z\,\boldsymbol{\rho}) + B_n W_n'(\boldsymbol{e}\cdot\boldsymbol{e}_z)\boldsymbol{e}\cdot\boldsymbol{\rho}(\boldsymbol{e}_z\cdot\boldsymbol{e}\,\boldsymbol{e}_z - \boldsymbol{e}). \tag{3.11}$$

The boundary conditions suggest that it would be wise to attempt to express the velocity and pressure as power series in $\varepsilon^{1/2}$. More precisely, we consider the following expansions:

$$\left.\begin{array}{ll} u = u_0 + \varepsilon^{1/2}u_1 + O(\varepsilon), & v = v_0 + \varepsilon^{1/2}v_1 + O(\varepsilon), \\ w = \varepsilon^{1/2}w_0 + \varepsilon w_1 + O\left(\varepsilon^{3/2}\right), & p = \varepsilon^{-3/2}p_0 + \varepsilon^{-1}p_1 + O\left(\varepsilon^{-1/2}\right), \end{array}\right\} \tag{3.12}$$

where $\boldsymbol{u} = (u, v, w)$ and all the functions in (3.12) are independent of ε. Note that to satisfy the boundary conditions the terms in these power series must differ by $O(\varepsilon^{1/2})$ rather than the $O(\varepsilon)$ that is required to solve the equivalent problem of a translating or rotating rigid sphere.

3.1. *The first-order solution*

Integrating the z-component of the first equation in (3.4) shows that $p_0 = p_0(X, Y)$, which is as yet an arbitrary function (assumed to have continuous second partial derivatives). The following solutions for u_0 and v_0 can be found by integrating the x- and y-components:

$$u_0 = \frac{1}{2}\frac{\partial p_0}{\partial X}(Z - H_1)(Z - H_2) + \frac{Z - H_2}{H}\boldsymbol{u}_0\cdot\boldsymbol{e}_x, \tag{3.13}$$

$$v_0 = \frac{1}{2}\frac{\partial p_0}{\partial Y}(Z - H_1)(Z - H_2) + \frac{Z - H_2}{H}\boldsymbol{u}_0\cdot\boldsymbol{e}_y. \tag{3.14}$$

Here

$$H = H_1 - H_2 = 1 + \frac{\alpha + 1}{2\alpha}\rho^2 + O(\varepsilon), \tag{3.15}$$

is the distance between the two spheres' surfaces at $\boldsymbol{\rho}$ from their line of centres (see figure 3). Using the equation of continuity, these solutions can be combined to yield

$$\frac{H^3}{12}\nabla_\perp^2 p_0 + \frac{H^2}{4}\frac{\alpha + 1}{\alpha}\boldsymbol{\rho}\cdot\nabla_\perp p_0 - \frac{\alpha - 1}{2\alpha}\sum_n B_n W_n(-\boldsymbol{e}\cdot\boldsymbol{e}_z)\boldsymbol{e}\cdot\boldsymbol{\rho} = 0. \tag{3.16}$$

We seek a solution to (3.16) of the form

$$p_0(\rho, \phi) = q_0(\rho)\,\boldsymbol{e}\cdot\boldsymbol{e}_\rho \tag{3.17}$$

and find that q_0 satisfies a linear second-order ordinary differential equation in one variable, ρ:

$$\frac{H^3}{12\rho^2}\frac{\partial}{\partial\rho}\left(\rho\frac{\partial q_0}{\partial\rho}\right) - \frac{H^3}{12\rho^3}q_0 + \frac{H^2}{4}\frac{\alpha + 1}{\alpha}\frac{\partial q_0}{\partial\rho} - \sum_n \frac{\alpha - 1}{2\alpha}B_n W_n(-\boldsymbol{e}\cdot\boldsymbol{e}_z) = 0. \tag{3.18}$$

This is the Reynolds equation for the problem (see Kim & Karrila 1992). The solution for the particular integral of (3.18) is

$$q_0 = -\frac{6\rho}{5H^2}\frac{\alpha-1}{\alpha+1}\sum_n B_n W_n(-\boldsymbol{e}\cdot\boldsymbol{e}_z). \tag{3.19}$$

The boundary conditions on the function p_0 are that it must tend to a constant as $\rho \to \infty$ and must be bounded and single-valued at $\rho = 0$ (which implies that $q_0 = 0$ on $\rho = 0$, from (3.17)).

One can now apply some simple asymptotics to find the leading-order behaviour of the function q_0. For $\rho \ll 1$ the complementary function acts like $q_0 \sim \rho^{\pm 1}$. The negative power must be discounted since q_0 would not then be finite in the limit $\rho \to 0$. Likewise for $\rho \gg 1$ it can be shown that $q_0 \sim \rho^{-(3\pm\sqrt{10})}$. This time the positive root, $\sqrt{10}-3$, can be discounted since q_0 must be bounded in the limit $\rho \to \infty$. Thus if there exists a non-trivial component of the complementary solution it must have the following asymptotic behaviour:

$$q_0(\rho) \sim \begin{cases} R_1\rho, & \rho \ll 1, \\ R_2\rho^{-(3+\sqrt{10})}, & \rho \gg 1, \end{cases} \tag{3.20}$$

where R_1 and R_2 are constants. Now consider (3.18), ignoring the last term (which will be accounted for later, in the particular integral). If the function $q_0 \sim R_1\rho$ for $\rho \ll 1$, and $q_0 \to 0$ as $\rho \to \infty$ and is non-trivial then, assuming that the constant of proportionality is positive near the origin ($R_1 > 0$), there must exist at least one maximum. Consider this point first. Here $\partial q_0/\partial\rho = 0$ and $q_0 > 0$, which implies from (3.18) that $\partial^2 q_0/\partial\rho^2 > 0$; this is contradictory, however, since the point is a maximum (and it does not occur at $\rho = 0$). Likewise if R_1 is negative the same argument can be made for the first minimum. Hence there cannot be any contribution to q_0 from the complementary function, since it cannot satisfy both boundary conditions. The asymptotic behaviour of the particular integral can also be calculated, and the following behaviour is found:

$$q_0 = \begin{cases} -\dfrac{6}{5}\dfrac{\alpha-1}{\alpha+1}B_n W_n(-\boldsymbol{e}\cdot\boldsymbol{e}_z)(\rho^3 + O(\rho^5)), & \rho \ll 1, \\ -\dfrac{6}{5}\dfrac{\alpha-1}{\alpha+1}\left(\dfrac{\alpha+1}{2\alpha}\right)^{-2} B_n W_n(-\boldsymbol{e}\cdot\boldsymbol{e}_z)\left(\dfrac{1}{\rho^3} + O(\rho^{-5})\right), & \rho \gg 1. \end{cases} \tag{3.21}$$

For confirmation the solution was calculated numerically and showed the same asymptotic behaviour. Thus the numerical solution confirms that there is no contribution from the complementary solution.

There are points of consequence about the function q_0: (*a*) if $\alpha = 1$ there is no pressure difference from that outside the lubrication region, and hence the flow is Couette; (*b*) if $\alpha - 1 \ll 1$ then the pressure function scales with $\alpha - 1$, the non-dimensional difference in size of the squirmers; (*c*) the theory is actually valid for all values of α (if one is more delicate with the asymptotic expansions, one can show this). Therefore very small spheres next to big spheres can be covered by this theory, as well as a sphere near a wall (where $\alpha \gg 1$ but, as can be observed, the pressure remains bounded and is $O(1)$).

3.2. *The forces and torques on squirmer* 1

Calculating the forces on the two spheres is an essential prerequisite to calculating the velocity difference. It is only by demanding that the spheres are force and torque

free that their solid-body motions can be calculated. To find the force we first rewrite the velocities slightly. In a frame such that $\boldsymbol{e}\cdot\boldsymbol{e}_y=0$ the velocities of the spheres given in (3.13) and (3.14) can be rewritten (using the expression for $\boldsymbol{u}_0$ given in (3.10)) to give the ϕ-dependence explicitly. We write $\boldsymbol{e}$ in Cartesian coordinates as

$$\boldsymbol{e}=e_1\boldsymbol{e}_x+e_3\boldsymbol{e}_z, \tag{3.22}$$

where $e_1^2+e_3^2=1$. The leading-order fluid velocity in the gap is

$$\boldsymbol{e}_\rho\cdot\left(\frac{1}{2}\nabla q_0(Z-H_1)(Z-H_2)+\frac{Z-H_1}{H}\boldsymbol{u}_0\right), \tag{3.23}$$

in the ρ-direction, where ρ,ϕ,Z are cylindrical coordinates (defined in the standard way from the Cartesian coordinates). Re-expressing (3.23) using (3.22) gives the velocity component in the ρ-direction as

$$\begin{aligned}&\boldsymbol{e}_\rho\cdot\left(\frac{1}{2}\nabla(q_0e_1\cos\phi)(Z-H_1)(Z-H_2)-\frac{Z-H_1}{H}\sum_n B_nW_n(-\boldsymbol{e}\cdot\boldsymbol{e}_z)\boldsymbol{e}\right)\\&\quad=\boldsymbol{e}\cdot\boldsymbol{e}_\rho\left(\frac{1}{2}\frac{\partial q_0}{\partial\rho}(Z-H_1)(Z-H_2)-\frac{Z-H_1}{H}\sum_n B_nW_n(-\boldsymbol{e}\cdot\boldsymbol{e}_z)\right)\end{aligned} \tag{3.24}$$

and the velocity component in the ϕ-direction as

$$\boldsymbol{e}\cdot\boldsymbol{e}_\phi\left(\frac{1}{2}\frac{q_0}{\rho}(Z-H_1)(Z-H_2)-\frac{Z-H_1}{H}\sum_n B_nW_n(-\boldsymbol{e}\cdot\boldsymbol{e}_z)\right). \tag{3.25}$$

Now the force integrand can be calculated; for example, if $\mathrm{d}F_x$ is a force element in the x-direction then

$$\mathrm{d}F_x=\boldsymbol{e}_x\cdot[\boldsymbol{\sigma}\cdot\boldsymbol{n}]\,\mathrm{d}A, \tag{3.26}$$

where $\boldsymbol{\sigma}$ is the stress tensor. Furthermore,

$$\boldsymbol{e}_x\cdot[\boldsymbol{\sigma}\cdot\boldsymbol{n}]=-p\,\boldsymbol{n}\cdot\boldsymbol{e}_x+2\mu\{(\boldsymbol{e}_\rho\cdot\boldsymbol{n})(\mathscr{E}_{\rho\rho}\boldsymbol{e}_\rho+\mathscr{E}_{\phi\rho}\boldsymbol{e}_\phi)+(\boldsymbol{e}_z\cdot\boldsymbol{n})(\mathscr{E}_{\rho z}\boldsymbol{e}_\rho+\mathscr{E}_{\phi z}\boldsymbol{e}_\phi)\}\cdot\boldsymbol{e}_x, \tag{3.27}$$

where $\mathscr{E}$ is the rate of strain tensor. So, expressing the ϕ-dependence explicitly yields

$$\begin{aligned}\mathrm{d}F_x=-\Bigg\{&\frac{\mu}{a}q_0\sin\theta\cos\phi\,\boldsymbol{e}\cdot\boldsymbol{e}_\rho\\&+\mu\left[2\frac{\partial u_{0,\rho}}{\partial\rho^*}\sin\theta\cos\phi\,\boldsymbol{e}\cdot\boldsymbol{e}_\rho-\left(\frac{\partial u_{0,\phi}}{\partial\rho^*}\boldsymbol{e}\cdot\boldsymbol{e}_\phi+\frac{1}{\rho^*}u_{0,\rho}\boldsymbol{e}\cdot\boldsymbol{e}_\phi\right)\sin\theta\sin\phi\right.\\&\left.-\left(\frac{\partial u_{0,\rho}}{\partial z}+\frac{\partial u_{0,z}}{\partial\rho^*}\right)\cos\theta\cos\phi\,\boldsymbol{e}\cdot\boldsymbol{e}_\rho+\left(\frac{1}{\rho^*}u_{0,z}\boldsymbol{e}\cdot\boldsymbol{e}_\phi+\frac{\partial u_{0,\phi}}{\partial z}\boldsymbol{e}\cdot\boldsymbol{e}_\phi\right)\cos\theta\sin\phi\right]\Bigg\}\,\mathrm{d}A.\end{aligned} \tag{3.28}$$

Equation (3.28) is given in terms of the unscaled coordinates ρ^*,z and the ϕ-independent components $u_{0,\rho},u_{0,\phi}$ and $u_{0,z}$ are defined by

$$u_{0,\rho}(\rho,z)\,\boldsymbol{e}\cdot\boldsymbol{e}_\rho=\boldsymbol{u}_0\cdot\boldsymbol{e}_\rho,\quad u_{0,\phi}(\rho,z)\,\boldsymbol{e}\cdot\boldsymbol{e}_\phi=\boldsymbol{u}_0\cdot\boldsymbol{e}_\phi,\quad u_{0,z}(\rho,z)\,\boldsymbol{e}\cdot\boldsymbol{e}_\rho=\varepsilon^{1/2}w_0. \tag{3.29}$$

The ϕ-dependence of w_0 in (3.29) is found by integrating the continuity equation at zero order in ε, using (3.13) and (3.14).

Defining new functions Q_0 and v_M such that

$$Q_0 \sum_n B_n W_n(-\boldsymbol{e}\cdot\boldsymbol{e}_z) = q_0 \tag{3.30}$$

and

$$v_M \sum_n B_n W_n(-\boldsymbol{e}\cdot\boldsymbol{e}_z) = u_M, \quad \forall \text{ subscripts } M, \tag{3.31}$$

in order to non-dimensionalise velocities and pressures, gives the expression for the force integrand (3.28), integrated over the ϕ-coordinate from 0 to 2π, as

$$\begin{aligned}\int_0^{2\pi} \mathrm{d}F_x\,\mathrm{d}\phi = \int \mu\pi a \sum_n B_n W_n(-\boldsymbol{e}_z\cdot\boldsymbol{e})\boldsymbol{e}\cdot\boldsymbol{e}_x \\ \times\Bigg\{-\varepsilon^{-3/2}Q_0\sin\theta - \Bigg[2\varepsilon^{-1/2}\frac{\partial v_{0,\rho}}{\partial\rho}\sin\theta - \varepsilon^{-1/2}\left(\frac{\partial v_{0,\phi}}{\partial\rho}\sin\theta\frac{1}{\rho}v_{0,\rho}\right) \\ -\left(\varepsilon^{-1}\frac{\partial v_{0,\rho}}{\partial Z} + \varepsilon^{-1/2}\frac{\partial v_{0,z}}{\partial\rho}\right)\cos\theta \\ -\left(\frac{1}{\rho}v_{0,z} + \varepsilon^{-1}\frac{\partial v_{0,\phi}}{\partial Z}\right)\cos\theta\Bigg]\Bigg\}\sin\theta\,\mathrm{d}\theta.\end{aligned} \tag{3.32}$$

The asymptotic behaviour of Q_0 can be calculated from the governing equation of the pressure, (3.18), subject to the boundary conditions that $q_0 = 0$ when $\rho = 0$ and $q_0 \ll 1$ for $\rho \gg 1$. Thus

$$Q_0 = \begin{cases} R\rho - \left(\dfrac{3}{8}R - \dfrac{3}{2}\right)\dfrac{\alpha-1}{2\alpha}\rho^3 + O(\rho^5), & \rho \ll 1, \\ -\dfrac{12}{5}\dfrac{\alpha-1}{2\alpha}\left(\dfrac{\alpha+1}{2\alpha}\right)^{-3}\rho^{-3} + O(\rho^{-5}), & \rho \gg 1, \end{cases} \tag{3.33}$$

where R is a constant. In the gap region $\pi - \theta \ll 1$, and this suggests the change of variables $\rho = \varepsilon^{-1/2}\sin\theta$, which implies that

$$\mathrm{d}\rho = \varepsilon^{-1/2}\sqrt{1-\varepsilon\rho^2}\,\mathrm{d}\theta. \tag{3.34}$$

This gives the leading-order force on sphere A as

$$F_x = \mu\pi a\boldsymbol{e}\cdot\boldsymbol{e}_x \sum_n B_n W_n(-\boldsymbol{e}\cdot\boldsymbol{e}_z)\int_0^{\rho_0}\left\{-Q_0\rho^2 + \left(\frac{1}{2}H\,(Q_0\rho)' - \frac{2}{H}\right)\right\}\mathrm{d}\rho, \tag{3.35}$$

where ρ_0 corresponds to the limit of the lubrication region. The two terms in the integrand are both $O(\rho^{-1})$ for $\rho \gg 1$. These integrals can be evaluated analytically. The force is then (asymptotically for large ρ_0) calculated from (3.35) to give

$$F_x = \frac{8}{5}\mu\pi a\frac{\alpha(2\alpha^2+\alpha+2)}{(1+\alpha)^3}\sum_n B_n W_n(-\boldsymbol{e}\cdot\boldsymbol{e}_z)\left(\log\rho_0^2 + O(1)\right). \tag{3.36}$$

One should now match the inner solution with the outer one to find a value for ρ_0. As discussed by O'Neill & Stewartson (1967), a precise assignment of ρ_0 is not required; instead a matching procedure is used. The above inner solution is matched in the limit of large ρ_0 with corresponding entity from the outer solution. For a consistent result

$$\rho_0 = \frac{D}{\varepsilon^{1/2}}, \tag{3.37}$$

where $D \sim O(1)$ is determined from the outer solution. Therefore, since

$$\log \rho_0 = -\frac{1}{2}\log \varepsilon + \log D,$$
$$\sim -\frac{1}{2}\log \varepsilon, \tag{3.38}$$

the force can be expressed from (3.36) in terms of ε:

$$F_x = -\frac{8}{5}\mu\pi a \boldsymbol{e}\cdot\boldsymbol{e}_x \frac{\alpha(2\alpha^2+\alpha+2)}{(1+\alpha)^3}\sum_n B_n W_n(-\boldsymbol{e}\cdot\boldsymbol{e}_z)(\log\varepsilon + O(1)), \tag{3.39}$$

which to leading order is independent of the flow field outside the lubrication region. This is analogous to the flow generated by a rigid sphere moving past a second sphere in a direction perpendicular to their line of centres (e.g. Kim & Karrila 1992).

The force element in the z-direction, dF_z, must be given by

$$\mathrm{d}F_z = \boldsymbol{e}_z\cdot[\boldsymbol{\sigma}\cdot\boldsymbol{n}]\,\mathrm{d}A,$$
$$= \left(-\frac{\mu}{a}q_0\boldsymbol{e}_z\cdot\boldsymbol{n}\cdot\mathscr{E}^*_{z\rho}\boldsymbol{e}_\rho\cdot\boldsymbol{n} + \mathscr{E}^*_{zz}\boldsymbol{e}_z\cdot\boldsymbol{n}\right)\mathrm{d}A. \tag{3.40}$$

However, to leading order in ϕ all the terms in (3.40) are proportional to $\boldsymbol{e}\cdot\boldsymbol{e}_\rho$ and hence $\cos\phi$ (and are otherwise independent of ϕ) and so integrate to zero. It follows that the force in the z-direction will be such that (cf. Kim & Karrila 1992, § 9.3)

$$F_z = O(-\log\varepsilon). \tag{3.41}$$

The torque exerted on sphere 1 will now be calculated in the same way. One can find an expression for the total torque independent of the flow outside the lubrication region:

$$T_y = -\frac{4\alpha(\alpha+4)}{5(\alpha+1)^2}\mu\pi a^2 \boldsymbol{e}\cdot\boldsymbol{e}_x \sum_n B_n W_n(-\boldsymbol{e}\cdot\boldsymbol{e}_z)(\log\varepsilon + O(1)). \tag{3.42}$$

By symmetry $T_x = 0$. The torque element in the z-direction, $\mathrm{d}T_z$, can also be calculated, as follows:

$$\mathrm{d}T_z = \boldsymbol{n}\cdot\boldsymbol{e}_x\mathrm{d}F_y - \boldsymbol{n}\cdot\boldsymbol{e}_y\mathrm{d}F_x$$
$$= \sin\theta\cos\phi\left(\mathscr{E}^*_{\rho\rho}\boldsymbol{e}_y\cdot\boldsymbol{e}_\rho\boldsymbol{e}_\rho\cdot\boldsymbol{n} + \mathscr{E}^*_{\phi\rho}\boldsymbol{e}_y\cdot\boldsymbol{e}_\phi\boldsymbol{e}_\rho\cdot\boldsymbol{n} + \mathscr{E}^*_{\rho z}\boldsymbol{e}_y\cdot\boldsymbol{e}_\rho\boldsymbol{e}_z\cdot\boldsymbol{n} + \mathscr{E}^*_{\phi z}\boldsymbol{e}_y\cdot\boldsymbol{e}_\phi\boldsymbol{e}_z\cdot\boldsymbol{n}\right)$$
$$-\sin\theta\sin\phi\left(\mathscr{E}^*_{\rho\rho}\boldsymbol{e}_x\cdot\boldsymbol{e}_\rho\boldsymbol{e}_\rho\cdot\boldsymbol{n} + \mathscr{E}^*_{\phi\rho}\boldsymbol{e}_x\cdot\boldsymbol{e}_\phi\boldsymbol{e}_\rho\cdot\boldsymbol{n} + \mathscr{E}^*_{\rho z}\boldsymbol{e}_x\cdot\boldsymbol{e}_\rho\boldsymbol{e}_z\cdot\boldsymbol{n} + \mathscr{E}^*_{\phi z}\boldsymbol{e}_x\cdot\boldsymbol{e}_\phi\boldsymbol{e}_z\cdot\boldsymbol{n}\right). \tag{3.43}$$

Now every component of the rate of strain tensor (to leading order) is proportional to either $\sin\phi$ or $\cos\phi$, and every $\boldsymbol{e}_i\cdot\boldsymbol{e}_\rho$ or $\boldsymbol{e}_i\cdot\boldsymbol{e}_\phi$ (where $i = x, y$) is also proportional to $\sin\phi$ or $\cos\phi$. Therefore integrating any term in (3.43) over ϕ from 0 to 2π will give zero. Hence $T_z = O(\varepsilon)$. The force and torque on the static sphere 2 can also be calculated in the same way.

3.3. *The stresslet of squirmer* 1

Calculating the stresslet generated by two squirmers in a fluid otherwise at rest involves adding up two terms: (*a*) the stresslet caused by the squirming motion on the surface (without the translational–rotational velocities of the two spheres); (*b*) the stresslet due to the translational–rotational velocities of the two spheres, which is the same as that for inert spheres (Kim & Karrila 1992).

To calculate the stresslet due to squirming on either sphere, the tensor

$$\int_A \boldsymbol{n}\boldsymbol{\sigma}\cdot\boldsymbol{n}\,\mathrm{d}A, \tag{3.44}$$

needs to be evaluated. As the leading-order velocity on either sphere (which is $\boldsymbol{u}_0$ or $\boldsymbol{0}$) is constant within the lubrication region, we have, to that order,

$$\int_A (\boldsymbol{u}\boldsymbol{n}+\boldsymbol{n}\boldsymbol{u})\,\mathrm{d}A = \boldsymbol{0}, \tag{3.45}$$

where A is that part of either sphere's surface within the lubrication region. The integrand in (3.44) will be

$$\begin{aligned}\boldsymbol{n}\boldsymbol{\sigma}\cdot\boldsymbol{n} &= \boldsymbol{n}(-p_0^*\boldsymbol{n}+\mathscr{E}_{\rho\rho}\boldsymbol{e}_\rho\boldsymbol{e}_\rho\cdot\boldsymbol{n}+\mathscr{E}_{\rho z}\boldsymbol{e}_\rho\boldsymbol{e}_z\cdot\boldsymbol{n}+\mathscr{E}_{\phi\rho}\boldsymbol{e}_\phi\boldsymbol{e}_\rho\cdot\boldsymbol{n}\\ &\quad+\mathscr{E}_{\phi z}\boldsymbol{e}_\phi\boldsymbol{e}_z\cdot\boldsymbol{n}+\mathscr{E}_{z\rho}\boldsymbol{e}_z\boldsymbol{e}_\rho\cdot\boldsymbol{n}+\mathscr{E}_{zz}\boldsymbol{e}_z\boldsymbol{e}_z\cdot\boldsymbol{n}),\\ &= -q_0^*\boldsymbol{e}\cdot\boldsymbol{e}_\rho\,\boldsymbol{n}\boldsymbol{n}+\boldsymbol{n}\boldsymbol{e}_\rho(\mathscr{E}_{\rho\rho}\sin\theta+\mathscr{E}_{\rho z}\cos\theta),\\ &\quad+\boldsymbol{n}\boldsymbol{e}_\phi(\mathscr{E}_{\phi\rho}\sin\theta+\mathscr{E}_{\phi z}\cos\theta)+\boldsymbol{n}\boldsymbol{e}_z(\mathscr{E}_{z\rho}\sin\theta+\mathscr{E}_{zz}\cos\theta)\end{aligned} \tag{3.46}$$

where $\boldsymbol{n}=(\sin\theta\cos\phi,\ \sin\theta\sin\phi,\ \cos\theta)$ and q_0^* and p_0^* are dimensional pressure functions:

$$q_0^* = \varepsilon^{-3/2}\frac{\mu}{a}q_0, \quad p_0^* = \varepsilon^{-3/2}\frac{\mu}{a}p_0. \tag{3.47}$$

Furthermore one can note that the following strain-rate components,

$$\mathscr{E}_{\rho\rho}, \quad \mathscr{E}_{\rho z}, \quad \mathscr{E}_{zz}, \quad \mathscr{E}_{z\rho}, \tag{3.48}$$

and the pressure term are linearly dependent on $\boldsymbol{e}\cdot\boldsymbol{e}_\rho$. The following components are proportional to $\boldsymbol{e}\cdot\boldsymbol{e}_\phi$:

$$\mathscr{E}_{\phi\rho}, \quad \mathscr{E}_{\phi z}, \quad \mathscr{E}_{\rho\phi}, \quad \mathscr{E}_{z\phi}, \quad \mathscr{E}_{\phi\rho}. \tag{3.49}$$

Other than these dependences all the components of $\mathscr{E}$ in (3.48) and (3.49) are independent of ϕ. Therefore the only non-zero components of (3.44), integrated over ϕ, are the ρz-, ϕz-, $z\rho$- and $z\phi$- components.

Before proceeding, we will take note of the order (in terms of ε) of the pressure term, and then this term will be shown to be asymptotically smaller than the leading-order behaviour of the terms derived from the rate of strain tensor. First, the pressure term is

$$-Q_0\boldsymbol{n}\,\boldsymbol{n}\,\boldsymbol{e}\cdot\boldsymbol{e}_\rho \tag{3.50}$$

times a dimensional factor

$$\mu\varepsilon^{-3/2}a^{-1}\sum_n B_n W_n(-\boldsymbol{e}\cdot\boldsymbol{e}_z). \tag{3.51}$$

Since

$$\boldsymbol{e}\cdot\boldsymbol{e}_\rho = \boldsymbol{e}\cdot(\cos\phi\,\boldsymbol{e}_x+\sin\phi\,\boldsymbol{e}_y) = e_1\cos\phi, \tag{3.52}$$

the term given in (3.50) can be integrated over ϕ from 0 to 2π. This leaves only the ρz, $z\rho$ terms non-zero and equal to $\pi e_1 Q_0\sin^2\theta\cos\theta$. In the integration region we have $\rho=\varepsilon^{-1/2}\sin\theta$, and so the integrand of this part of the stresslet will be $O(\varepsilon)$ multiplied by $\sin\theta\,\mathrm{d}\theta$, which is $O(\varepsilon)$, and then multiplied by $O(\varepsilon^{-3/2})$ (the factor multiplying pressure), giving a leading-order contribution for this term of $O(\varepsilon^{1/2})$. Furthermore, since $\boldsymbol{e}\cdot\boldsymbol{e}_y=0$ the ϕ-integral of (3.46) (except for the pressure term) can

be evaluated:

$$\int_0^{2\pi} \boldsymbol{n}\boldsymbol{\sigma}\cdot\boldsymbol{n}\,\mathrm{d}\phi = \pi \boldsymbol{e}_z\boldsymbol{e}_x\cos\theta\,\boldsymbol{e}\cdot\boldsymbol{e}_x(\mathscr{E}'_{\rho\rho}\sin\theta + \mathscr{E}'_{\rho z}\cos\theta + \mathscr{E}'_{\phi\rho}\sin\theta + \mathscr{E}'_{\phi z}\cos\theta) + \pi\boldsymbol{e}_x\boldsymbol{e}_z\sin\theta\,\boldsymbol{e}\cdot\boldsymbol{e}_x(\mathscr{E}'_{z\rho}\sin\theta + \mathscr{E}'_{zz}\cos\theta). \tag{3.53}$$

Now, in the same way as for the force calculation, (3.53) needs to be integrated over the θ-direction too. Rather than performing this directly, we note that the integration region will be such that $\rho = \varepsilon^{-1/2}\sin\theta$, and so in these coordinates (3.53) becomes

$$\int \boldsymbol{n}\boldsymbol{\sigma}\cdot\boldsymbol{n}\mathrm{d}A = \mu\pi a\boldsymbol{e}_z\boldsymbol{e}_x\,\boldsymbol{e}\cdot\boldsymbol{e}_x\int_0^{\rho_0}\left[\frac{\partial u'_{0,\rho}}{\partial Z} + \frac{\partial u'_{0,\phi}}{\partial Z}\right]_{Z=H_1}\rho\,\mathrm{d}\rho + O(\varepsilon). \tag{3.54}$$

Then substituting the results for $u_{0,\rho}$ and $u_{0,\phi}$ from (3.24) and (3.25), respectively, gives

$$\int \boldsymbol{n}\boldsymbol{\sigma}\cdot\boldsymbol{n}\mathrm{d}A = \mu\pi a\boldsymbol{e}_z\boldsymbol{e}_x\,\boldsymbol{e}\cdot\boldsymbol{e}_x\int_0^{\rho_0}\sum_n B_n W_n(-\boldsymbol{e}\cdot\boldsymbol{e}_z)\left[\frac{1}{2}(Q_0\rho)' - \frac{2\rho}{H}\right]\mathrm{d}\rho + O(\varepsilon), \tag{3.55}$$

which by similar asymptotic means gives the following result:

$$\begin{aligned}\int \boldsymbol{n}\boldsymbol{\sigma}\cdot\boldsymbol{n}\mathrm{d}A &= \mu\pi a\boldsymbol{e}_z\boldsymbol{e}_x\,\boldsymbol{e}\cdot\boldsymbol{e}_x\sum_n B_n W_n(-\boldsymbol{e}\cdot\boldsymbol{e}_z)\left(\frac{4\alpha(\alpha+4)}{5(\alpha+1)^2}\log\rho_0^2 + O(1)\right)\\ &= -\mu\pi a\boldsymbol{e}_z\boldsymbol{e}_x\,\boldsymbol{e}\cdot\boldsymbol{e}_x\sum_n B_n W_n(-\boldsymbol{e}\cdot\boldsymbol{e}_z)\left(\frac{4\alpha(\alpha+4)}{5(\alpha+1)^2}\log\varepsilon + O(1)\right).\end{aligned} \tag{3.56}$$

Once again this is independent of D, where

$$\rho_0 = \frac{D}{\varepsilon^{1/2}}. \tag{3.57}$$

Writing $\boldsymbol{e}_z = \boldsymbol{\xi}/\xi$ (where $\boldsymbol{\xi}$ is the vector from the point on sphere 1 closest to sphere 2 to the point on sphere 2 closest to sphere 1) to conform with the notation used by Batchelor & Green (1972*a*) one can express the stresslet as

$$\boldsymbol{S} = \int \boldsymbol{n}\boldsymbol{\sigma}\cdot\boldsymbol{n}\,\mathrm{d}A = -\mu\pi a\,\frac{4\alpha(\alpha+4)}{5(\alpha+1)^2}\sum_n B_n W_n\left(-\frac{\boldsymbol{e}\cdot\boldsymbol{\xi}}{\xi}\right)\log\varepsilon \times\frac{\boldsymbol{\xi}}{\xi}\left(\boldsymbol{e} - \frac{\boldsymbol{e}\cdot\boldsymbol{\xi}}{\xi}\frac{\boldsymbol{\xi}}{\xi}\right) + O(1). \tag{3.58}$$

The stresslet of the static sphere 2 can be calculated in the same way.

4. Comparison between analytical results and numerical simulation

It is not clear how applicable the above analyses for far- and near-field separation are for intermediate particle separations. The intermediate-distance flow properties will be computed using a boundary-element method (BEM), as first developed by Youngren & Acrivos (1975), and the results will be compared with the analytical results. In this section, and the remainder of the paper, we show only the results for two identical spheres, i.e. $\alpha = 1$ and $\boldsymbol{B}^{(1)} = \boldsymbol{B}^{(2)}$, with only two squirming modes, B_1 and B_2 ($B_n = 0$ for $n > 2$). Of course the orientations of the two squirmers, $\boldsymbol{e}_1$ and $\boldsymbol{e}_2$, are in general different.

4.1. *Numerical methods*

When there are N squirmers in an infinite fluid, the Stokes flow field external to the squirmers can be given in integral form as

$$\boldsymbol{u}(\boldsymbol{x}) = \boldsymbol{u}^{\infty}(\boldsymbol{x}) - \sum_{m=1}^{N} \int_{A'_m} \boldsymbol{K}(\boldsymbol{x} - \boldsymbol{x}') \cdot \boldsymbol{q}(\boldsymbol{x}') \, \mathrm{d}A'_m \tag{4.1}$$

where $\boldsymbol{u}^{\infty}$ is the undisturbed velocity, i.e. the flow field without particles, A_m is the surface of squirmer m and $\boldsymbol{K}$ is the Oseen tensor. The single-layer potential $\boldsymbol{q}$ is found by subtracting the traction force on the inner surface, $\boldsymbol{f}_{in}$, from that on the outer surface, $\boldsymbol{f}_{out}$:

$$\boldsymbol{q} = \boldsymbol{f}_{out} - \boldsymbol{f}_{in}. \tag{4.2}$$

The boundary condition is given by

$$\boldsymbol{u}(\boldsymbol{x}) = \boldsymbol{U}_m + \boldsymbol{\Omega}_m \wedge (\boldsymbol{x} - \boldsymbol{x}_m) + \boldsymbol{u}_{s,m}, \quad \boldsymbol{x} \in A_m, \tag{4.3}$$

where $\boldsymbol{U}_m$ and $\boldsymbol{\Omega}_m$ are the translational and rotational velocities of squirmer m. $\boldsymbol{x}_m$ is the centre of squirmer m and $\boldsymbol{u}_{s,m}$ is the squirming velocity of squirmer m, defined by (A 8).

Equation (4.1) with the boundary condition (4.3) expresses the velocity field generated by point forces in a homogeneous fluid and is not restricted to a rigid-body motion inside a squirmer. In order to impose a rigid-body motion, one needs to introduce a double-layer potential in (4.1) and to deal with velocity slip on the surface explicitly. Introducing double-layer potentials, however, considerably increases the computational load. Since $\boldsymbol{f}_{in}$ can be obtained analytically in the case of a squirmer, it is computationally more efficient to express the velocity field in terms of single-layer potentials alone rather than using two kinds of potential. The effect of $\boldsymbol{f}_{in}$ appears in calculating the stresslet of a squirmer, so it is subtracted analytically, as explained in Appendix B. The boundary-element method using single- or double-layer potentials only, the so-called generalized boundary-integral method, is explained in detail, with a derivation of the integral equations and the force and torque exerted on a particle, in the established text Pozrikidis (1992).

It is supposed that squirmer m is subjected to known external forces $\boldsymbol{F}_m$ and torques $\boldsymbol{T}_m$. The equilibrium conditions for squirmer m are

$$\boldsymbol{F}_m = \int_{A_m} \boldsymbol{q}(\boldsymbol{x}) \, \mathrm{d}A_m, \tag{4.4}$$

$$\boldsymbol{T}_m = \int_{A_m} \boldsymbol{x} \wedge \boldsymbol{q}(\boldsymbol{x}) \, \mathrm{d}A_m. \tag{4.5}$$

Squirmers are assumed to be neutrally buoyant, so $\boldsymbol{F}_m = 0$. The centre of buoyancy of the squirmer may not coincide with its geometric centre (see figure 2), and in that case the torque $\boldsymbol{T}_m$ is given by (2.6). The stresslet of squirmer m can be expressed using the single-layer potential as

$$\boldsymbol{S}_m = \int_{A_m} \left[\frac{1}{2} (\boldsymbol{q}\boldsymbol{x} + \boldsymbol{x}\boldsymbol{q}) - \frac{1}{3} \boldsymbol{x} \cdot \boldsymbol{q} \boldsymbol{I} \right] \mathrm{d}A. \tag{4.6}$$

A detailed derivation of the stresslet is given in Appendix B.

These governing equations are non-dimensionalized using the radius a, the swimming velocity of a solitary squirmer, $2B_1/3$, and the fluid viscosity μ. Let the ratio of second-mode squirming to first-mode squirming be β, i.e. $\beta = B_2/B_1$. In

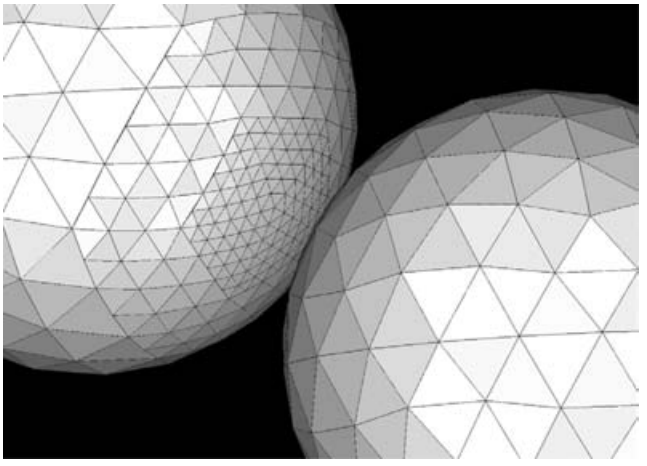

FIGURE 4. Boundary elements on the surface of squirmers. Smaller triangles are generated in the near-contact region, when $\varepsilon \leqslant 0.1$.

the case of a bottom-heavy squirmer, its behaviour is determined by a dimensionless parameter G_{bh} given by

$$G_{bh} = \frac{2\pi\rho g a h}{\mu B_1}. \tag{4.7}$$

G_{bh} is the ratio of the gravitational torque to the viscous-drag torque.

The boundary-element method is employed to discretize (4.1). By evaluating (4.1) at M distinct boundary points, a system of $3M$ linear algebraic equations will result and can be written in matrix form as

$$\{\boldsymbol{u} - \boldsymbol{u}^{\infty}\} = [\mathscr{A}]\{\boldsymbol{\tau}\}, \tag{4.8}$$

where $[\mathscr{A}]$ is a fully populated $3M \times 3M$ matrix. The boundary condition (4.3) and the equilibrium conditions (4.4) and (4.5) can also be written in matrix form as:

$$\{\boldsymbol{u}\} = [\mathscr{B}]\{\boldsymbol{U}, \boldsymbol{\Omega}\} + \{\boldsymbol{u}_s\} \tag{4.9}$$

and

$$[\mathscr{C}]\{\boldsymbol{\tau}\} = \{\boldsymbol{F}, \boldsymbol{T}\}, \tag{4.10}$$

respectively. $[\mathscr{B}]$ is a $6 \times 3M$ matrix and $[\mathscr{C}]$ is a $3M \times 6$ matrix. Finally, by combining all three equations, the linear algebraic equations for the problem can be written as

$$\left[\begin{array}{c|c} \mathscr{A} & -\mathscr{B} \\ \hline \mathscr{C} & 0 \end{array}\right] \left\{\begin{array}{c} \boldsymbol{\tau} \\ \hline \boldsymbol{U}, \boldsymbol{\Omega} \end{array}\right\} = \left\{\begin{array}{c} \boldsymbol{u}_s - \boldsymbol{u}^{\infty} \\ \hline \boldsymbol{F}, \boldsymbol{T} \end{array}\right\}. \tag{4.11}$$

When the minimum separation of the squirmers ε is larger than 0.1 (distance being non-dimensionalized by the radius a), the surface of a single squirmer is divided into 320 nearly equal-sized triangles. When $\varepsilon \leqslant 0.1$, smaller triangles are generated in the near-contact region, as shown in figure 4, in order to reduce numerical errors. The total number of triangles in this case is 590 per squirmer. The integration in (4.1) is performed on a triangle element by using 28-point Gaussian polynomials (Lyness & Jespersen 1975). The singularity in the integration at $x = 0$ is solved analytically

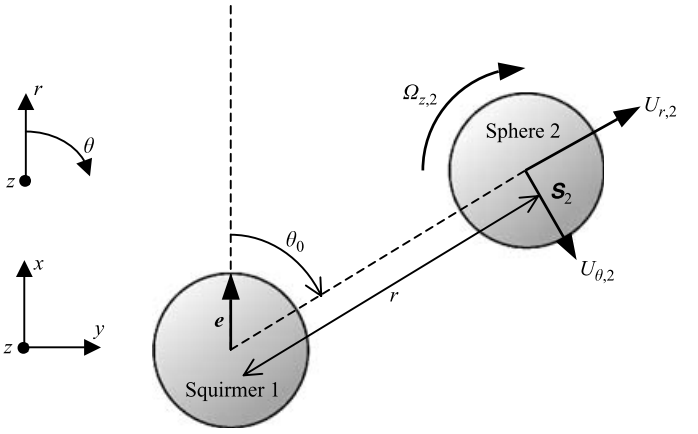

FIGURE 5. Diagram of the geometry for squirmer 1 and sphere 2. The squirming motion of squirmer 1 generates a translational velocity (with components $U_{r,2}$ and $U_{\theta,2}$), (a) rotational velocity $\Omega_{z,2}$ and a stresslet $\boldsymbol{S}_2$ on sphere 2; θ_0 is the angle between the orientation vector $\boldsymbol{e}$ of squirmer 1 and $\boldsymbol{r}$.

(Youngren & Acrivos 1975). The linear algebraic equation (4.11) is solved by LU decomposition, including pivoting. In § 5 the trajectories of two squirmers are obtained, where the time marching is performed by the Runge–Kutta–Fehlberg method. This method is a combination of fourth- and sixth-order Runge–Kutta schemes, and the time step is determined step by step according to an error criterion.

Though BEM has no limitation in dealing with the boundary condition (4.3), we omit squirming modes higher than the second mode, i.e. $B_n = 0$ in $\boldsymbol{u}_{s,m}$ when $n \geqslant 3$, as stated above. If one wants to prescribe an infinite series of squirming modes on the surface, one needs to generate an infinite number of infinitely small boundary elements on the surface. In the numerical simulation, therefore, we cannot technically deal with high modes of squirming velocity. The reasons for limiting ourselves to the first and second modes are: (*a*) in the case of a solitary squirmer, the first mode determines the swimming speed, the second mode determines the stresslet and the higher modes have no effect on the swimming speed or the stresslet; (*b*) the higher a mode is, the more rapidly it decays with r, so the effect of higher modes is negligible in the far-field interaction; (*c*) the effect of high modes in the near field is to generate fluctuations in the velocities and stresslet due to small displacements in the θ-direction. The overall properties, such as the trajectories of a pair of squirmers, may be captured by using the first few modes. This simplification in the boundary condition for the BEM is used throughout this paper.

4.2. *Comparison for far-field separation*

Let squirmer 1 be at the centre of a cylindrical coordinate system with orientation vector $\boldsymbol{e}$ and $\beta = 1$ ($B_2 = B_1$). Let sphere 2, which has no squirming velocity, be at $\boldsymbol{r}$ with the same radius as squirmer 1. Let the $z = 0$ plane contain $\boldsymbol{e}$ and the centres of both squirmers; let θ_0 be the angle between the orientation vector $\boldsymbol{e}$ of squirmer 1 and $\boldsymbol{r}$. This coordinate system is illustrated in figure 5. The squirming motion of squirmer 1 generates a translational velocity (with components $U_{r,2}$ and $U_{\theta,2}$), a rotational velocity $\Omega_{z,2}$ and a stresslet $\boldsymbol{S}_2$ on sphere 2. These quantities are compared with the analytical results. If one wants to know the velocities and stresslet generated by two squirmers, one just needs to add up two cases, (i) particle 1 is a squirmer and

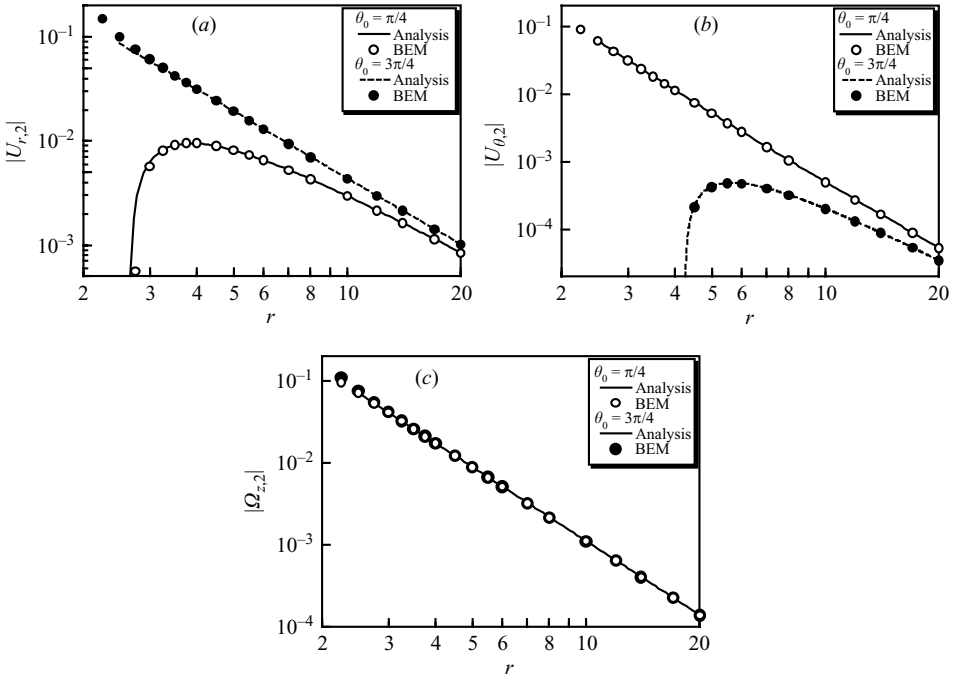

FIGURE 6. Comparison of the translational–rotational velocities of sphere 2 at $\theta_0 = \pi/4$ and $3\pi/4$. Here 'analysis' stands for the analytical results and 'BEM' stands for the numerical results using the boundary-element method. (*a*) The translational velocity in the r-direction, $U_{r,2}$, (*b*) the translational velocity in the θ-direction, $U_{\theta,2}$, (*c*) the rotational velocity, $\Omega_{z,2}$.

particle 2 is an inert sphere and (ii) particle 1 is an inert sphere and particle 2 is a squirmer, because the flow problem is linear. We will also neglect bottom-heaviness throughout this section, i.e. we will take $G_{bh} = 0$. The effect of bottom-heaviness is simple to include, and one just needs to superimpose the additional rotational velocity and asymmetric part of the stress tensor caused by the bottom-heaviness.

For far-field separation, the translational–rotational velocities can be given as (2.3) and (2.7), respectively. These analytical equations will now be compared with the numerical results using BEM. Figures 6(*a*) and 6(*b*) show a comparison of the translational velocity components of sphere 2 in the r- and θ- directions $U_{r,2}$ and $U_{\theta,2}$, respectively, for $\theta_0 = \pi/4$ and $3\pi/4$. We see that the analytical and numerical results correspond well even when $r < 3$, so (2.3) is applicable over quite a wide range of r values. At leading order $U_{r,2}$ decays as r^{-2} and $U_{\theta,2}$ decays as r^{-3}, and this is confirmed by the numerical results. Figure 6(*c*) shows the comparison for the rotational velocity $\Omega_{z,2}$ of sphere 2, for $\theta_0 = \pi/4$ and $3\pi/4$. The absolute values of the rotational velocities in these two cases are the same in the far field, so the two cases overlap in the figure. It is found that the analytical and numerical results correspond very well even when $r < 2.5$. At leading order $\Omega_{z,2}$ decays as r^{-3}, and again this is confirmed by the numerical results.

The difference between the analysis and the numerical simulation for translational–rotational velocities was examined at various values of θ_0. The difference for $U_{r,2}$ is generally larger than for $U_{\theta,2}$ or $\Omega_{z,2}$; therefore only the result for $U_{r,2}$ is shown in figure 7. The difference is defined by the absolute value of the analytical velocity $U_{r,2}^{ana}$ minus the numerical velocity $U_{r,2}^{BEM}$. It is found that this velocity difference is lower

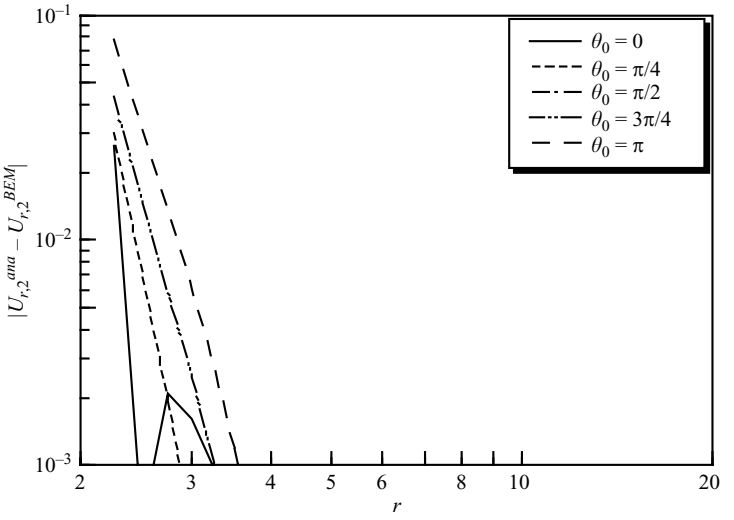

FIGURE 7. The difference between the analysis and the numerical simulation for the translational velocity in the r-direction, $U_{r,2}$, at various values of θ_0. The difference is defined by the absolute value of the analytical velocity $U_{r,2}^{ana}$ minus the numerical velocity $U_{r,2}^{BEM}$.

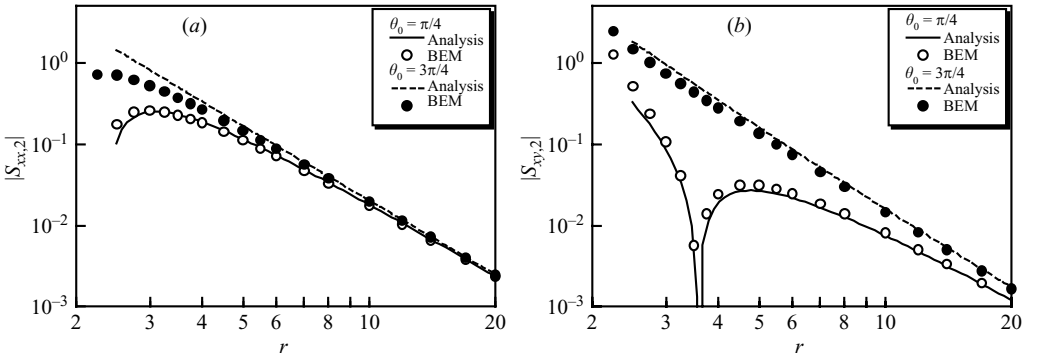

FIGURE 8. Comparison of the stresslet on sphere 2 at $\theta_0 = \pi/4$ and $3\pi/4$. Here 'analysis' stands for the analytical results and 'BEM' stands for the numerical results using the boundary-element method. (*a*) The stresslet component $S_{xx,2}$, (*b*) the stresslet component $S_{xy,2}$.

than 10^{-2} if $r > 3$. Therefore the analytical equations (2.3) and (2.7) can be used for $r \geqslant 3$ with an accuracy of approximately 1%.

The stresslet can be given as (2.9) in the far field. Figures 8(*a*) and 8(*b*) show a comparison of the stresslet components $S_{xx,2}$ and $S_{xy,2}$ on sphere 2; for $\theta_0 = \pi/4$ and $3\pi/4$. Here the x-axis is taken in the $\boldsymbol{e}$-direction and the y-axis is taken in the $\theta_0 = \pi/2$ direction, as illustrated in figure 5. It is found that the analytical and numerical results again correspond well when $r > 3$, though not quite as well as for the velocities. At leading order, the stresslet decays as r^{-3}, which is confirmed by the numerical results.

The difference between the analysis and the numerical simulation for the stresslet was examined at various values of θ_0, and the results are shown in figures 9(*a*) and 9(*b*). The strength of the stresslet for a solitary squirmer is of order 10, so the difference itself is rather larger than for the translational velocity (figure 7). The difference decreases to below 10^{-1} when $r \geqslant 4.0$ and 10^{-2} when $r \geqslant 6$. If sphere 2 is

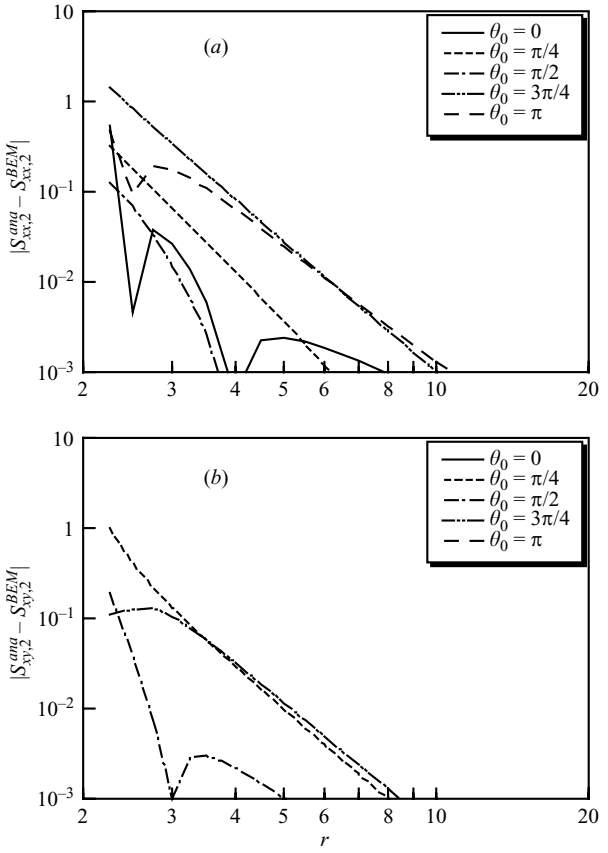

FIGURE 9. The difference in stresslet $\boldsymbol{S}_2$ between the analysis and the numerical simulation with various θ_0 conditions. The difference is defined by the absolute value of the analytical stresslet $\boldsymbol{S}_2^{ana}$ minus the numerical stresslet $\boldsymbol{S}_2^{BEM}$. (*a*) The stresslet component $S_{xx,2}$, (*b*) the stresslet component $S_{xy,2}$.

far enough from squirmer 1, the stresslet $S_{xx,1}$ generated by squirmer 1 equals 4π, from (A 14). If one bases the relative error in the stresslet on this value, one may say that the analytical equation (A 14) can be used for $r \geqslant 3.5$ with an accuracy of approximately 1%.

4.3. *Comparison for near-field separation*

When two squirmers are in near contact, the minimum separation ε between the two surfaces becomes very small. The boundary-element method needs very careful treatment in order to achieve high accuracy in such cases. As in former benchmark simulations (Ingber & Mammoli 1999 or Tran-Cong & Phan-Thien 1989, for instance), fine elements must be generated in the near-contact region (see figure 4). These fine elements do improve the numerical accuracy but, nevertheless, reliable results are not obtained when $\varepsilon < 0.01$. The comparison between the analysis and the numerical simulation was, therefore, performed mainly in the $\varepsilon \geqslant 0.01$ regime. The accuracy in the near field was checked by comparison with the analytical and exact solutions for two rigid spheres; the results will be shown later.

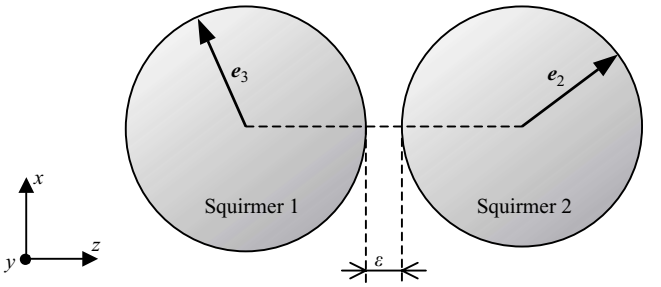

FIGURE 10. Diagram of the geometry for two near-separated squirmers at the minimum separation ε. Squirmers 1 and 2 have orientation vectors $\boldsymbol{e}_1$ and $\boldsymbol{e}_2$, respectively. The z-axis passes through the two squirmer centres, and Cartesian coordinates are taken.

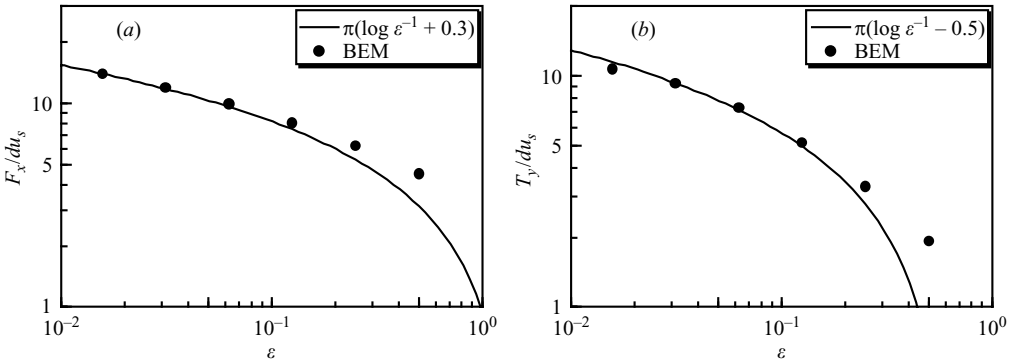

FIGURE 11. The force and torque generated by the shearing motion of two squirmers; 'BEM' stands for the numerical results using the boundary-element method. (*a*) The ratio of F_x and du_s, (*b*) the ratio of T_y and du_s.

Let the two squirmers, 1 and 2 say, have orientation vectors $\boldsymbol{e}_1$ and $\boldsymbol{e}_2$ respectively. Let them have the same radius, and the same squirming sets $\boldsymbol{B}$ with $\beta = 1$. Let the z-axis pass through the two squirmer centres, and Cartesian coordinates be taken as illustrated in figure 10. Although neither of $\boldsymbol{e}_1$ and $\boldsymbol{e}_2$ are necessarily in the (x, z)-plane, we have restricted them to lie in the (x, z)-plane for simplicity. When $\boldsymbol{e}_1 = (1, 0, 0)$ and $\boldsymbol{e}_2 = (-1, 0, 0)$ the squirmers swim past each other perpendicularly to their line of centres; this will be referred to as a shearing motion hereafter. When $\boldsymbol{e}_1 = (0, 0, 1)$ and $\boldsymbol{e}_2 = (0, 0, -1)$ they approach each other; this will be referred to as a squeezing motion. When $\boldsymbol{e}_1 = (1, 0, 0)$ and $\boldsymbol{e}_2 = (1, 0, 0)$ they swim in parallel; this will be referred to as a parallel motion. These three cases are dealt with in this section.

The force in the x-direction F_x and the torque in the y-direction T_y are derived as in (3.39) and (3.42), respectively, and they are proportional to the velocity difference on the surface and vary as $\log \varepsilon$ at leading order. In the case of a shearing motion of two identical squirmers, the non-dimensionalized equations (3.39) and (3.42) can be simplified to

$$F_x = \pi \mathrm{d}u_s(\log \varepsilon^{-1} + O(1)), \tag{4.12}$$

$$T_y = \pi \mathrm{d}u_s(\log \varepsilon^{-1} + O(1)), \tag{4.13}$$

where $\mathrm{d}u_s$ is the difference between the squirming velocities of the two squirmers at the minimum separation point. These analytical equations are compared with the numerical results using BEM in figures 11(*a*) and 11(*b*). We see both that the

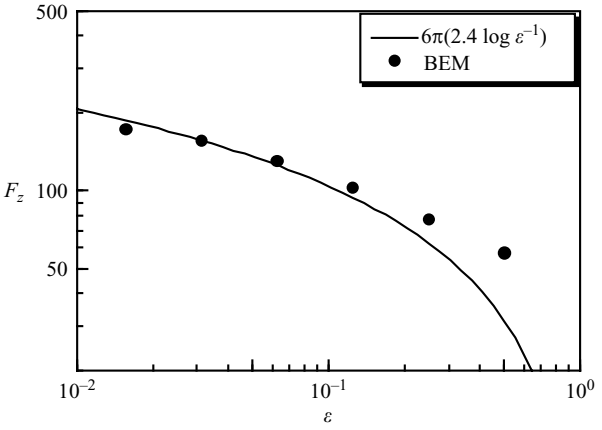

FIGURE 12. The force generated by the squeezing motion of two squirmers; 'BEM' stands for the numerical results using the boundary-element method.

analytical equations fit well with the numerical results and that the leading order of F_x and T_y is $\log \varepsilon^{-1}$ as predicted. In the case of shearing motion, the $O(1)$ term in (4.12) is 0.3 and that in (4.13) is -0.5 (these values are chosen for a good fit to the numerical results in figures 11(a) and 11(b)). Although (3.39) is analogous to a shearing force between two inert spheres, the $O(1)$ term in (4.12) is different from the value of 3.8 obtained in that case (e.g. Kim & Karrila 1992). This difference may come from the different velocity distributions of an inert sphere surface, given by a rigid-body motion, and a squirmer surface, given by the squirming velocity. The leading-order term $\log \varepsilon^{-1}$ is a weak singularity and thus dominates the solution only in the mathematical sense. The next-order, $O(1)$, term is always necessary and should be obtained by fitting with the numerical results.

The force in the z-direction, F_z, is $O(\log \varepsilon^{-1})$ at leading order, as given in (3.41). The numerical results for F_z in a squeezing motion and the fitted curve are shown in figure 12. This confirms that F_z is $O(\log \varepsilon^{-1})$ at leading order. By fitting the analytical equations to the numerical results at small ε, say $\varepsilon = 0.01$, one could obtain more accurate forces and torques in the $\varepsilon < 0.01$ range. This technique will be used in subsequent sections.

Solving the motion of two swimming squirmers without bottom-heaviness in a fluid otherwise at rest can be divided into the following two processes: (i) calculation of the force and torque generated by the squirming motion on the surface (without the translational–rotational velocities of two squirmer bodies) and (ii) calculation of the translational–rotational velocities of two inert spheres due to the force and torque obtained in (i). Again this is permitted because the problem is linear in the velocity field. Thus the relation between the torque due to squirming (without translational–rotational velocities) and the rotational velocity of a torque-free squirmer should be the same as that between the torque and the rotational velocity for two rigid spheres. This has been confirmed in the parallel-motion case, and the result is shown in figure 13. The reason why we chose the case of parallel motion is that both asymptotic (Kim & Karrila 1992) and exact (Goldman, Cox & Brenner 1966) solutions for two rigid spheres are available in this case. It is found that the ratio of the torque due to squirming, T_y^{squ}, and the rotational velocity Ω_y agrees with the analytical and exact solutions for the two-rigid-sphere case. Therefore, calculation (ii) can be done by

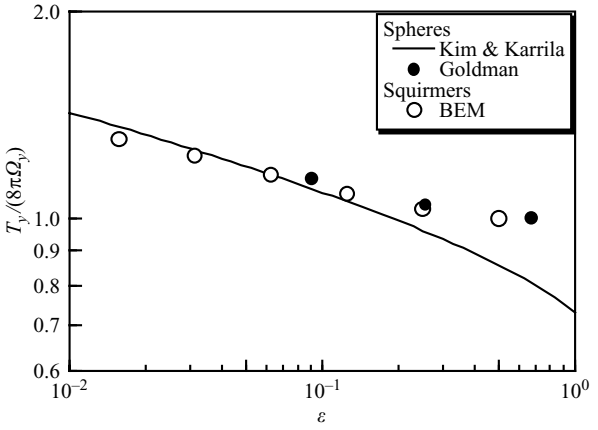

FIGURE 13. The ratio of the torque T_y and the rotational velocity Ω_y in a parallel-motion case. The line gives the analytical results of Kim & Karrila (1992) for rigid spheres and the solid dots show the exact results of Goldman, Cox & Brenner (1966) for rigid spheres. 'BEM' stands for the numerical results using the boundary-element method, in which the torque due to squirming is calculated without translational–rotational velocities and the rotational velocity is calculated for a torque-free squirmer.

exploiting a former study (e.g. Kim & Karrila 1992) even though the results are now obtained for squirmers without translational–rotational velocities. We have already shown how to obtain accurately the forces and torques generated by squirming in the near field; it is now possible to solve for the motion of two swimming squirmers in the near field. Figure 13 also shows that the accuracy of the BEM is acceptable when $\varepsilon \geqslant 0.01$.

The stresslet $\boldsymbol{S}$ caused by the squirming motion is obtained from (3.58) and is proportional to the velocity difference on the surface and to $\log \varepsilon$ at leading order. In the case of a shearing motion of two identical squirmers, the xz-component of the non-dimensionalized stresslet, S_{xz}, can be given as

$$S_{xz} = -\pi \mathrm{d} u_s (\log \varepsilon^{-1} + O(1)). \tag{4.14}$$

This analytical equation is compared with the numerical results using BEM in figure 14. It is found that the analytical equation fits well with the numerical results and that the leading order of S_{xz} is $\log \varepsilon^{-1}$ as predicted. The $O(1)$ term in this case is -0.3, which is different from the value -0.98 for the case of two inert spheres (e.g. Kim & Karrila 1992). Again, the leading-order term $\log \varepsilon^{-1}$ is a weak singularity, so the next-order, $O(1)$, term should be obtained by fitting to the numerical results.

Fitting all components of the stresslet to the numerical results can be tedious, so a simplified method will be shown here. When two squirmers are near to contact, the stresslet given by (A 12) can be re-expressed at leading order as

$$\boldsymbol{S}^{squ} = \boldsymbol{F}^{squ} \boldsymbol{n}_0 - \tfrac{1}{3} \boldsymbol{F}^{squ} \cdot \boldsymbol{n}_0 \boldsymbol{I}, \tag{4.15}$$

where the use of (3.45) shows that the last term in (A 12) vanishes; $\boldsymbol{S}^{squ}$ and $\boldsymbol{F}^{squ}$ are the stresslet and force due to squirming and $\boldsymbol{n}_0$ is the position vector from the centre of the sphere to the minimum separation point. The validity of (4.15) has been checked for both a shearing motion and a squeezing motion, and the results are shown in figures 15(a) and 15(b). It is found that all the stresslet components agree

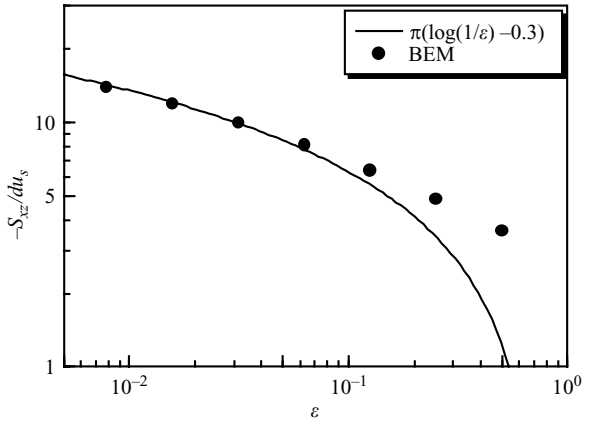

FIGURE 14. The ratio of the stresslet component S_{xz} and du_s in the case of a shearing motion of two squirmers; 'BEM' stands for the numerical results using the boundary-element method.

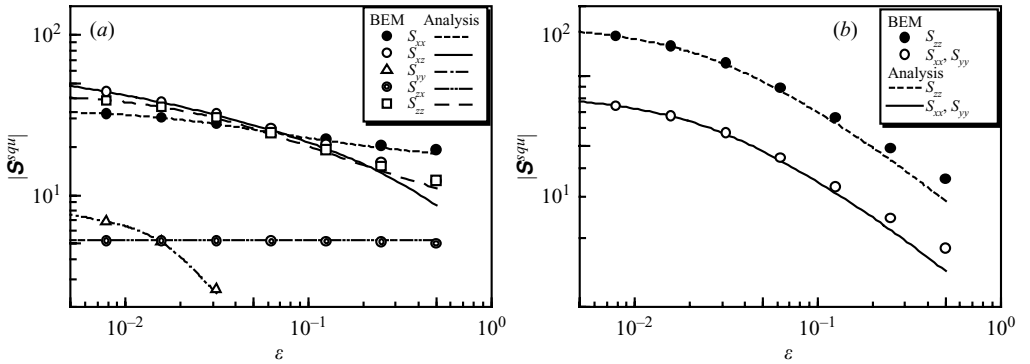

FIGURE 15. Comparison of stresslet components for the numerical results (BEM) and analytical results (analysis); the analytical results were calculated using the simplified equation (4.15) for the stresslet. (*a*) Two squirmers in a shearing motion, (*b*) two squirmers in a squeezing motion.

well with (4.15) in both cases when $\varepsilon < 0.1$. Since the force $\boldsymbol{F}^{squ}$ is proportional to $\log\varepsilon$ at leading order, the stresslet is also proportional to $\log\varepsilon$, as seen in (3.58). It is now possible to obtain all the stresslet components due to squirming by using a near-field expression for the force.

As mentioned previously, calculating the stresslet in the near field requires the addition of two terms: (i) the stresslet caused by the squirming motion and (ii) the stresslet due to the translational–rotational velocities of two inert spheres. The second stresslet, which is derived by subtracting the first stresslet from the total stresslet in the simulation, is shown, in figure 16, for a shearing motion in order to confirm the addition process and to check numerical accuracy. The analytical result for the second stresslet was calculated by assuming that two inert spheres move with the same translational–rotational velocities as in the two-squirmer simulation (Kim & Karrila 1992). It is found that the analytical and numerical results correspond well when $\varepsilon < 0.1$, so the validity of the addition process is confirmed. It is also found that the numerical accuracy for the stresslet is acceptable when $\varepsilon \geqslant 0.01$.

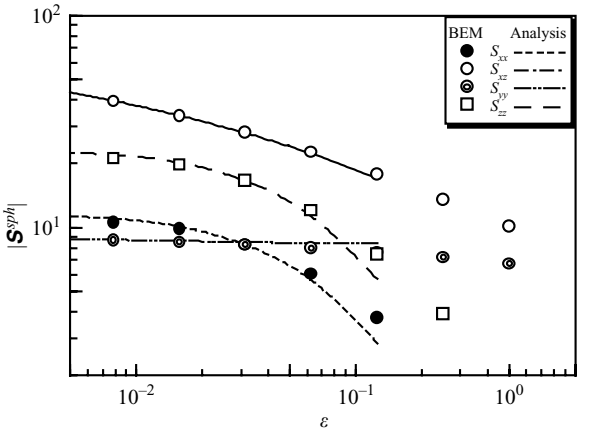

FIGURE 16. Stresslet due to the translational–rotational velocities of two inert spheres. The numerical result (BEM) was calculated by subtracting the stresslet due to squirming from the total stresslet, and the analytical result (Kim & Karrila) was calculated by assuming that two inert spheres move with the same translational–rotational velocities as in the two-squirmer simulation.

5. Trajectories of two squirmers

As explained in the introduction, it is intended that the results of this paper will be used to perform simulations of the trajectories of many squirmers in suspension, in order to assess the hydrodynamic effect of active squirming on macroscopic suspension properties, in the semi-dilute regime in which pairwise interactions dominate. Full boundary-element simulations of many squirmers would be prohibitively expensive, computationally, so in this section we compile a database of pairwise interactions, covering the whole range of relative initial positions and orientations of the two squirmers, from which an arbitrary interaction can be interpolated. On the way to compiling the database, we note a number of interesting features shown by the trajectories of just two interacting squirmers.

In the Stokes-flow regime, the motion of a squirmer and the flow field around it are determined instantaneously, because there is no inertia. Therefore, from arbitrary initial conditions one can calculate the trajectories of two squirmers by integrating the velocities in time. Rather than constructing a database of trajectories, which would require positions and orientations relative to their initial values, as functions of time, we will instead construct a database of the effective forces exerted by two squirmers on each other. The reasons for using forces are explained as follows. (i) Solving for the motion of two swimming squirmers in a fluid otherwise at rest can be divided into calculation of (*a*) the forces and torques generated by the squirming motion and (*b*) the velocities of two inert spheres due to these forces and torques. The motion of two spheres under given forces and torques has been studied extensively and a general outline of the method is included in standard texts (see, for instance, Kim & Karrila 1992). Therefore, if one has a database of the effective forces and torques generated by the squirming motion, one can easily calculate the velocities of the two squirmers. (ii) The database generated in this study describes the two-squirmer interaction only, though, as explained above, we intend to use it for a many-body simulation. If a suspension of squirmers is sufficiently dilute, the pairwise additivity

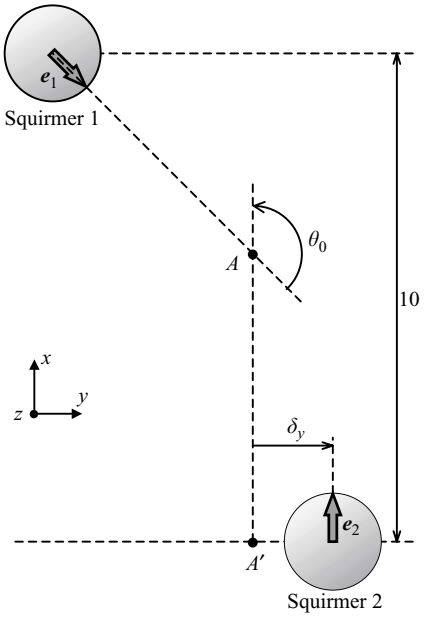

FIGURE 17. The geometry for the trajectories of squirmers 1 and 2. θ_0 is the angle between $\boldsymbol{e}_1$ and $\boldsymbol{e}_2$. Squirmer 1 is always placed 10 units apart from squirmer 2 in the x-direction, and the x-coordinate of point A relative to the centre of squirmer 2 is equal to the distance between point A and the centre of squirmer 1. The relative positions of A and A' from the centre of squirmer 1 can be uniquely determined as functions of θ_0. δ_y is the distance between the centre of squirmer 2 and point A'.

of either forces or velocities is valid. Generally speaking, the pairwise additivity of forces is to be preferred, because it can express lubrication forces more precisely and can be adjusted to prevent particles overlapping. (iii) The stresslet for both far- and near-field separation is known from (2.9) and (3.58), respectively. The near-field stresslet needs to be improved by using (4.15), which is possible if one has a database of forces.

In constructing the database we exploited the linearity of the flow problem and assumed that particle 1 is a squirmer and particle 2 is an inert sphere, as illustrated in figure 5. If one wants to know the forces and torques generated by two squirmers, one just needs to add the case where particle 1 is an inert sphere and particle 2 is a squirmer, which can be obtained from the same database. The database covers a wide range of relative positions such that $2.01 \leqslant r \leqslant 1000$ and $0 \leqslant \theta_0 \leqslant \pi$ (see figure 5). The results for $1000 < r$ and $r < 2.01$ can be calculated from the analytical results obtained in § 2 and § 3. The results for $\pi < \theta_0 < 2\pi$ can be obtained by exploiting the symmetry of the problem. The database covers the parameter range $0.1 \leqslant \beta \leqslant 10$ as well. Some sample lines are shown in table 1 for the case with $\beta = 1$; the total number of lines in this case is 54 481. The full database is available as a supplement to the online version of the paper.

In this section, we will introduce some interesting features of the trajectories. We begin by considering two-dimensional configurations, in which the centres and orientation vectors of the two squirmers are in the same plane. Let the x-direction be $\boldsymbol{e}_2$, and let the centre of squirmer 2 be placed δ_y apart from a point A' in the y-direction (see figure 17). Let point A be the intersection between the extension of $\boldsymbol{e}_1$

Line	$\theta_0\,(10^{-2})$	r	$F_{1,x}\,(10^2)$	$F_{1,y}$	$T_{1,z}$	$F_{2,x}\,(10^2)$	$F_{2,y}$	$T_{2,z}$
1	0.0000000	2.0100000	1.2174085	-3.1479160×10^{-14}	1.4528049×10^{-13}	−1.1099990	9.9733589×10^{-15}	-1.2322131×10^{-13}
2	1.7453293	2.0100000	1.2171774	1.2118332	6.8882938×10^{-1}	−1.1097651	−1.2251480	4.7030337
3	3.4906585	2.0100000	1.2161901	2.4179815	1.3768254	−1.1087570	−2.4444593	9.3993799
4	5.2359878	2.0100000	1.2144617	3.6162668	2.0635738	−1.1069900	−3.6557136	1.4085593
5	6.9813170	2.0100000	1.2120071	4.8045108	2.7486605	−1.1044795	−4.8566902	1.8758226
6	8.7266463	2.0100000	1.2088415	5.9805354	3.4316711	−1.1012409	−6.0451685	2.3413833
7	10.471976	2.0100000	1.2049798	7.1421622	4.1121917	−1.0972897	−7.2189279	2.8048969
⋮	⋮	⋮	⋮	⋮	⋮	⋮	⋮	⋮
182	0.0000000	2.0103915	1.2123818	-3.2934483×10^{-14}	1.4213806×10^{-13}	−1.1049766	7.1548602×10^{-15}	-1.2222647×10^{-13}
⋮	⋮	⋮	⋮	⋮	⋮	⋮	⋮	⋮
54481	314.15927	1009.0996	0.18803752	-2.7732075×10^{-10}	3.6425745×10^{-10}	−291.04566	6.7654162×10^{-10}	1.0440157×10^{-12}

TABLE 1. Sample lines of the database, in which particle 1 is a squirmer and particle 2 is an inert sphere. θ_0 and r are the angle and distance illustrated in figure 5. $F_{i,j}$ and $T_{i,j}$ are the jth components of the force and the torque exerted on particle i.

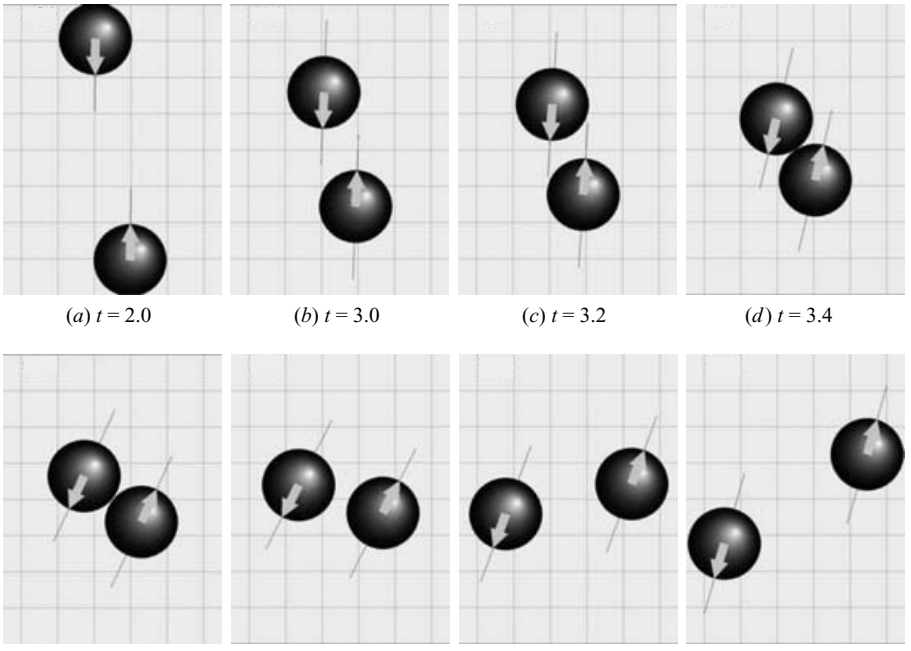

FIGURE 18. Sequences (*a*) to (*h*) show the interactions between two squirmers with $\beta = 5$ under the initial conditions $\theta_0 = \pi$ and $\delta_y = 1$.

from the centre of squirmer 1 and the extension of $\boldsymbol{e}_2$ from point A'. We restrict the configurations so that the x-coordinate of point A relative to the centre of squirmer 2 is equal to the distance between point A and the centre of squirmer 1. Initially, squirmer 1 is always placed a distance of 10 units from squirmer 2 in the x-direction, i.e. $r_{x,1} - r_{x,2} = 10$, where $r_{j,i}$ is the j-component of the positions vector of squirmer i. Then the relative positions of A and A' from the centre of squirmer 1 can be uniquely determined as functions of θ_0.

The value of the parameter β used in this section was 5, because the trajectories show more interesting features for higher values of β. Squirming modes higher than the second are omitted, as explained in § 4.1. Trajectories for any other value of β in the range $0.1 \leqslant \beta \leqslant 10$ can be readily calculated by using the database.

To start with, we show the interactions between two squirmers under the initial conditions $\theta_0 = \pi$ and $\delta_y = 1$ in figures 18(*a*) to 18(*h*) (see also movies 1 and 2). Here t is the dimensionless time and $t = 0$ is the initial instant. The orientation vectors of the squirmers are shown as big arrows on the spheres, and thin solid lines are added so that one can easily compare the angle between the two squirmers. It is found from the figure that the two squirmers come very close to each other, then change their orientation in the near field and finally move away from each other. The final directions of $\boldsymbol{e}_1$ and $\boldsymbol{e}_2$ are significantly different from the initial directions in this case. The trajectories of the two squirmers under the initial conditions $\theta_0 = \pi$ and $\delta_y = 1$, 2, 3, 5 or 10 are shown in figure 19. The arrows show the initial orientations of the squirmers. The interaction decreases with increasing $|\delta_y|$ and is small when $|\delta_y| \geqslant 10$. The change in the orientation vectors is significant only when the squirmers experience near contact.

Figures 20(*a*) to 20(*l*) show the interactions between two squirmers under the initial conditions $\theta_0 = \pi/2$ and $\delta_y = -5$ (see also movies 3 and 4). It is seen that they interact

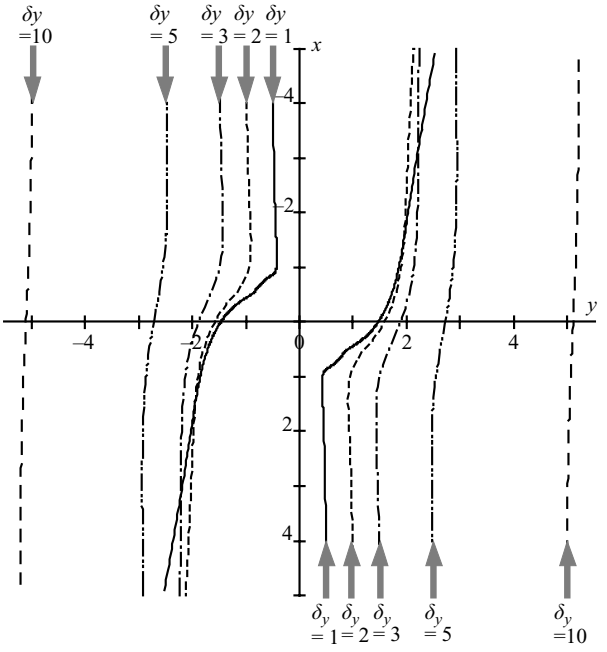

FIGURE 19. The trajectories of two squirmers under the initial conditions $\theta_0 = \pi$ and $\delta_y = 1$, 2, 3, 5 or 10 ($\beta = 5$).

strongly even though they are rather far apart initially ($\delta_y = -5$). The squirmers attract each other at first (see figure 20*b* for instance), then change their orientation in the near field (see figure 20*e*) and separate for a short distance (see figure 20*f*). However, they again attract each other (see figure 20*g*) and change their orientation in the near field (see figure 20*h*) but finally move away from each other. Their interaction is very complex and the final directions of $\boldsymbol{e}_1$ and $\boldsymbol{e}_2$ are completely different from the initial directions, in this case. The trajectories of two squirmers under the initial conditions $\theta_0 = \pi/2$ and $\delta_y = -1, -2, -3, -5$ or -10 are shown in figure 21. The interaction is very strong, and a change in the direction of $\boldsymbol{e}_2$ appears even when $\delta_y = -10$. The complexity of the trajectories may come from the disturbance of the flow field due to the region of closed streamlines behind a squirmer (see figure 1), because they often rotate as a pair when one squirmer is trapped behind the second.

Figures 22(*a*) to 22(*c*) show the interactions between two squirmers under the initial conditions $\theta_0 = \pi/4$ and $\delta_y = -1$ (see also movie 5). The basic behaviour of the two squirmers is completely different in this case. They come very close to each other at first, then change their orientation in the near field but do not escape from each other again. They swim as a pair, as shown in figure 22(*c*). We checked the stability of this pair-swimming motion by applying a disturbance to the original stable positions of the two squirmers. Let $\boldsymbol{r}_2^{stb}$ be the position of squirmer 2 relative to squirmer 1 when the squirmers are swimming steadily as a pair, in a two-dimensional configuration having the two squirmer centres, $\boldsymbol{e}_1$ and $\boldsymbol{e}_2$, in the same (x, y)-plane. First we applied a disturbance that retains the two-dimensionality and places squirmer 2 in the vicinity of the original position, at $\boldsymbol{r}_2^{stb} + \Delta\boldsymbol{r}_{xy}$, where $\Delta\boldsymbol{r}_{xy}$ is a vector in the (x, y)-plane with length 0.1. In this case, the displaced squirmer 2 tends to come back to its original position. Therefore the pair swimming motion is stable when they retain a two-dimensional configuration. Secondly, we applied the disturbance in the z-direction,

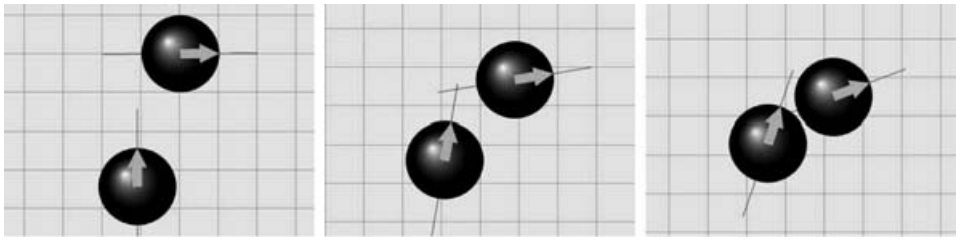

(*a*) $t = 6.0$ (*b*) $t = 7.0$ (*c*) $t = 7.5$

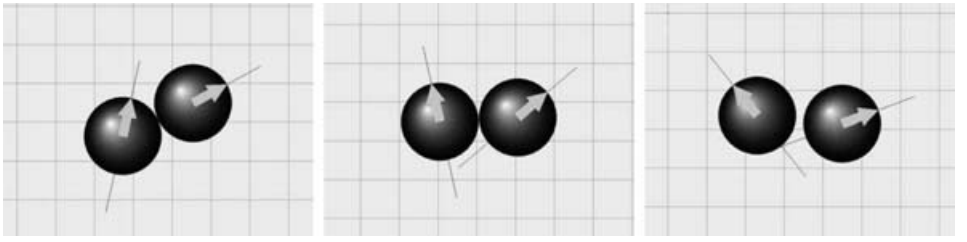

(*d*) $t = 7.75$ (*e*) $t = 8.25$ (*f*) $t = 9.0$

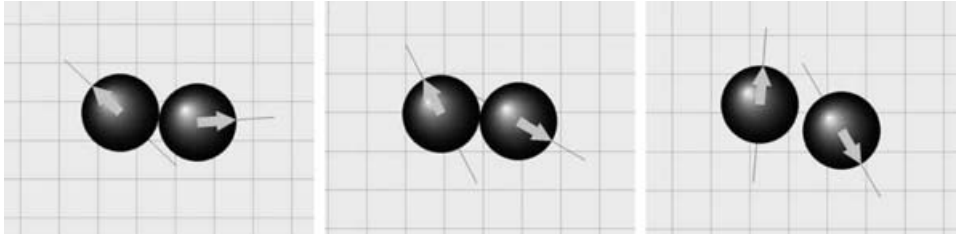

(*g*) $t = 9.5$ (*h*) $t = 10.25$ (*i*) $t = 11.0$

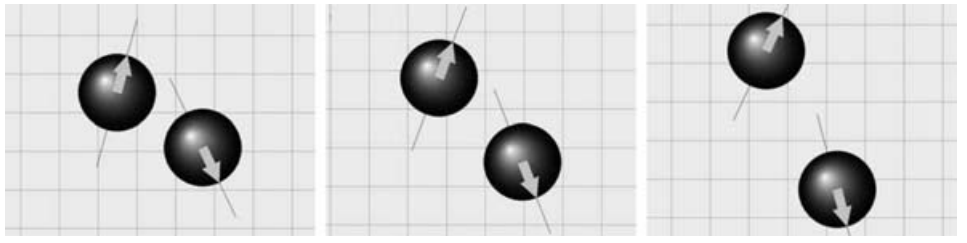

(*j*) $t = 11.5$ (*k*) $t = 12.0$ (*l*) $t = 13.0$

FIGURE 20. Sequences (*a*) to (*l*) show the interactions between two squirmers with $\beta = 5$ under the initial conditions $\theta_0 = \pi/2$ and $\delta_y = -5$.

placing squirmer 2 in the vicinity of the original position at $\boldsymbol{r}_2^{stb} + \Delta\boldsymbol{r}_z$, where $\Delta\boldsymbol{r}_z$ is a vector in the z-direction. In this case, the displaced squirmer 2 tends to move away from the original position for even a very small disturbance. Therefore the pair-swimming motion is unstable to three-dimensional disturbances.

The effect of three-dimensionality was investigated further, as follows. The vectors $\boldsymbol{e}_1$ and $\boldsymbol{e}_2$ are still within (x, y)-planes, but the two (x, y)-planes have a spacing of δ_z in the z-direction. The trajectories of two squirmers under the initial conditions $\theta_0 = \pi/4$, $\delta_y = -1$ and $\delta_z = 0$ or 0.1 are shown in figure 23. We see that the initial slight gap in the z-direction ($\delta_z = 0.1$) prevents the squirmers from swimming as a pair. The trajectories in these two cases are fully three-dimensional and the final directions

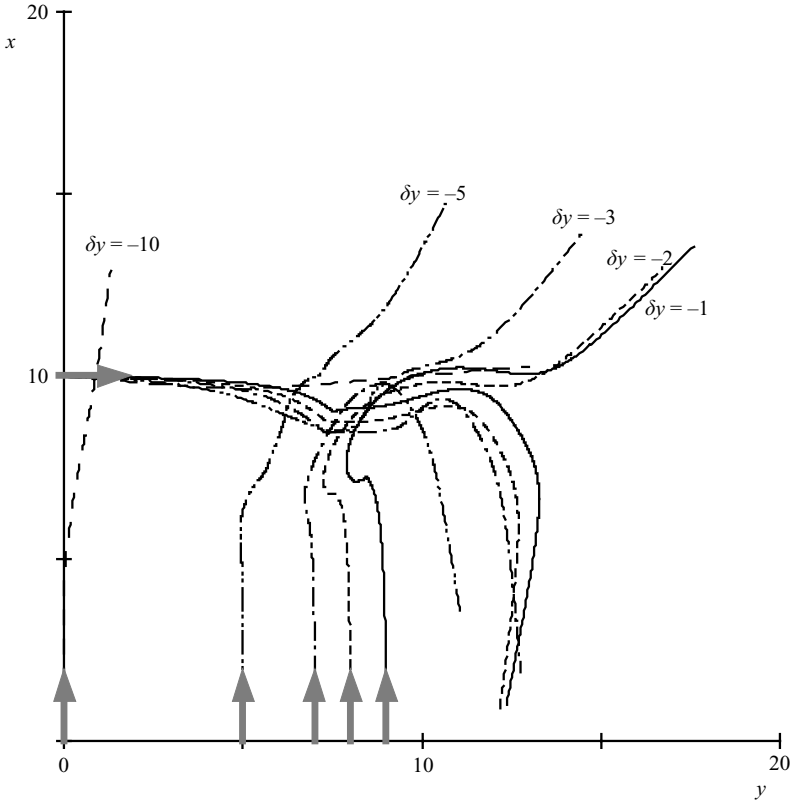

FIGURE 21. Trajectories of two squirmers under the initial conditions $\theta_0 = \pi/2$ and $\delta_y = -1$, -2, -3, -5 or -10 ($\beta = 5$).

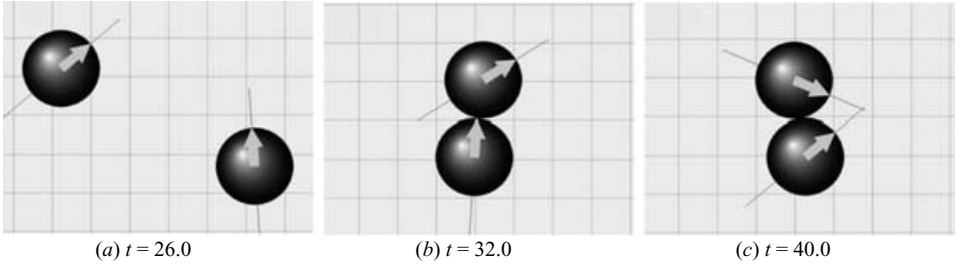

(*a*) $t = 26.0$ (*b*) $t = 32.0$ (*c*) $t = 40.0$

FIGURE 22. Sequences (*a*) to (*l*) show the interactions between two squirmers with $\beta = 5$ under the initial conditions $\theta_0 = \pi/4$ and $\delta_y = -1$.

of $\boldsymbol{e}_1$ and $\boldsymbol{e}_2$ are considerably different from the initial directions. The restriction to two-dimensional configurations is thus a very strong limitation, and in general the squirmer interactions should be treated three-dimensionally. Stable pairs are unlikely to be found in general.

However, the next example is necessarily two-dimensional. Figures 24(*a*) to 24(*f*) show the interactions between two squirmers under the initial conditions $\theta_0 = 0$ and $\delta_y = 1$ (see also movies 6 and 7). Although the two squirmers are swimming in the same direction, they attract each other at first, then change their orientation in the near field and finally move away from each other. The final directions of $\boldsymbol{e}_1$ and $\boldsymbol{e}_2$ are

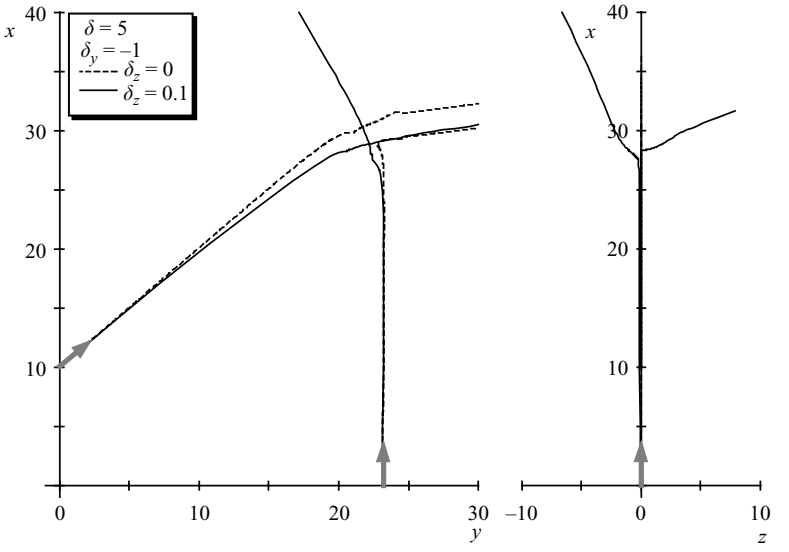

FIGURE 23. Effect of three-dimensional orientation on the trajectories of two squirmers with $\beta = 5$. $\boldsymbol{e}_1$ and $\boldsymbol{e}_2$ are each within an (x, y)-plane; however, the two (x, y)-planes have a gap of δ_z in the z-direction ($\theta_0 = \pi/4$, $\delta_y = -1$ and $\delta_z = 0$ or 0.1).

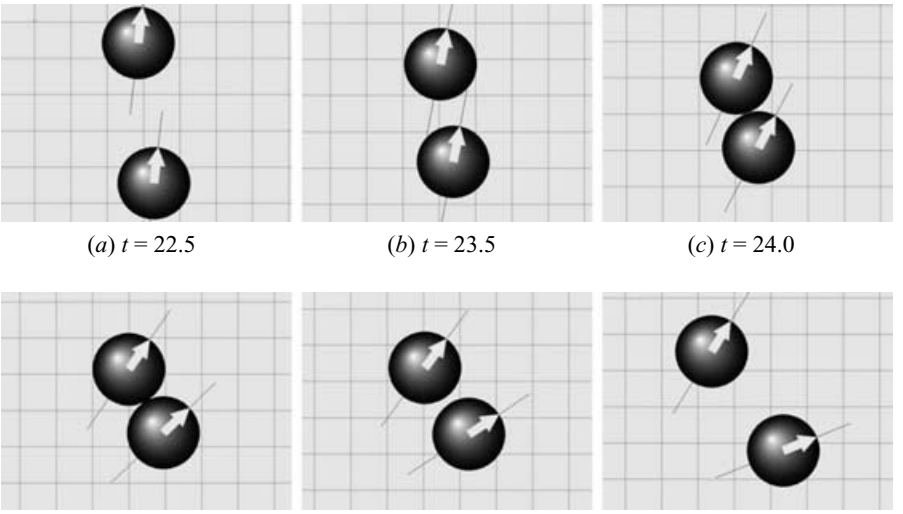

(*a*) $t = 22.5$ (*b*) $t = 23.5$ (*c*) $t = 24.0$

(*d*) $t = 24.25$ (*e*) $t = 24.5$ (*f*) $t = 25.5$

FIGURE 24. Sequences (*a*) to (*f*) show the interactions between two squirmers with $\beta = 5$ under the initial conditions $\theta_0 = 0$ and $\delta_y = 1$.

considerably different from the initial directions, and the two trajectories incline to the same direction. The trajectories of the two squirmers under the initial conditions $\theta_0 = 0$ and $\delta_y = 1$, 2, 3, 5 or 10 are shown in figure 25. In this case the two squirmers interact for a long time, because they are swimming in the same direction. Therefore, the effect of the interaction appears even when $\delta_y = 10$. All cases show a similar tendency, and the interaction is increased by decreasing δ_y.

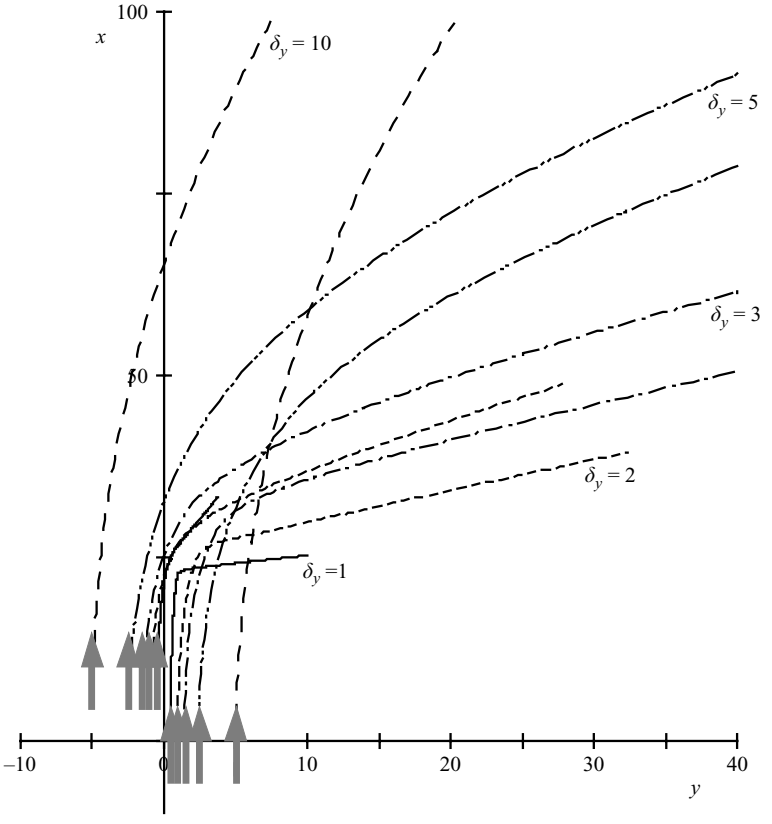

FIGURE 25. Trajectories of two squirmers under the initial conditions $\theta_0 = 0$ and $\delta_y = 1$, 2, 3, 5 or 10 ($\beta = 5$).

Lastly the effect of bottom-heaviness was investigated. The relevant parameter G_{bh} is defined in (4.7). If one assumes that the micro-organisms swim in water at 20 body lengths per second with their centre of mass a half-radius from the geometric centre, G_{bh} is about 5 for micro-organisms with radius 10 μm and about 50 for micro-organisms with radius 100 μm. The trajectories of two bottom-heavy squirmers under the initial conditions $\theta_0 = 0$ and $\delta_y = 5$ are shown in figure 26. Gravity acts in the $-x$-direction. The interaction in the near field inclines the trajectories to the right in all cases; however, the final direction is almost upwards if $G_{bh} \neq 0$. The two squirmers may come closer if G_{bh} is increased.

6. Summary and discussion

The interaction of two squirmers has been calculated analytically for the limits of small and large separation and has also been calculated numerically using a boundary-element method. In the far-field analysis, the translational–rotational velocities and the stresslet due to the interaction were derived, and the results correspond well with the numerical results. The analytical equations for the velocities, (2.3) and (2.7), can be used for $r \geqslant 3$ with an accuracy of approximately 1%. If one considers the error in the stresslet relative to the maximum stresslet component for a solitary squirmer, one may also say that the analytical equation (2.9) can be used for $r \geqslant 3.5$ with an accuracy of approximately 1%. In the near-field analysis, the forces, torques and

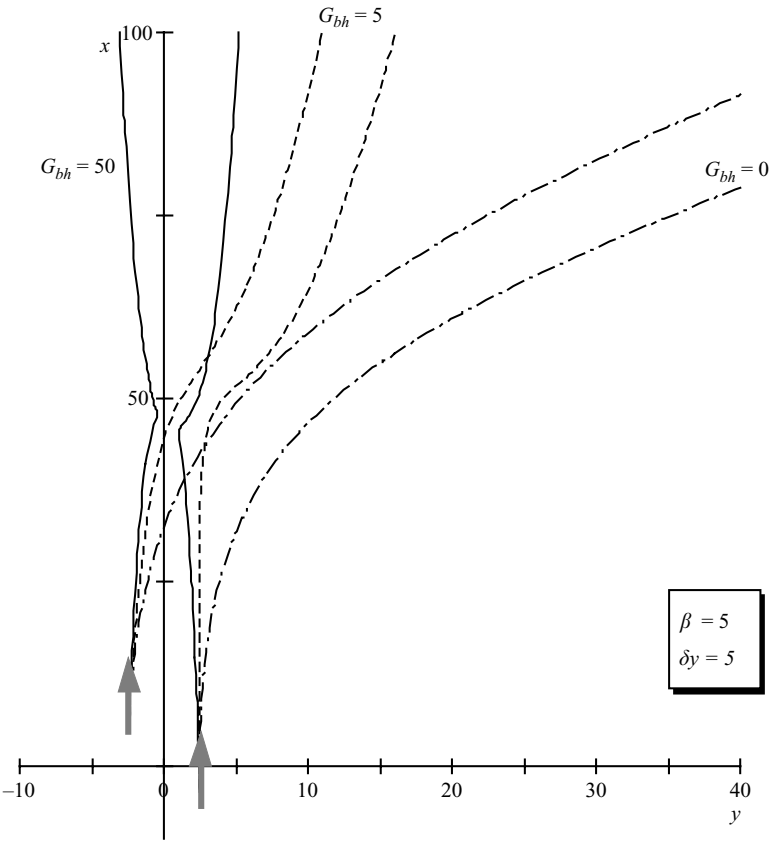

FIGURE 26. Effect of bottom-heaviness on the trajectories of two squirmers with $\beta = 5$ and $G_{bh} = 0$, 5 or 50. The initial condition is $\theta_0 = 0$ (two-dimensional orientation) and $\delta_y = 5$. Gravity acts in the $-x$-direction.

stresslets due to the interaction were derived, and again the results correspond well with the numerical results. The leading-order terms for these three quantities are of order $\log \varepsilon^{-1}$, which is a weak singularity. Thus the next-order term must be included; here it was obtained by fitting to the numerical results. Fitting all components of the stresslet to the numerical results may be tedious, so a simplified method was introduced in (4.15). The accuracy of this equation was confirmed by comparison with the numerical results.

We have generated a database for an interacting pair of squirmers so that squirmers' motion can be easily predicted. The database was constructed by calculating the forces generated by two squirmers on each other, covering the whole range of relative positions and orientations. The full database is available on the JFM website. The behaviour of two interacting squirmers was discussed phenomenologically, too. The results for the trajectories of two squirmers were shown for some interesting cases. The results show that the squirmers attract each other at first, then they change their orientation dramatically when they are in near contact and finally they separate from each other. The effect of bottom-heaviness is considerable. Restricting the trajectories to two dimensions is shown to give misleading results.

Throughout this paper the surface squirming velocity is assumed not to change during the interactions. Real micro-organisms, however, may well change their

swimming motion according to the presence of a nearby micro-organism. Of course, we have not modelled a cell's biological response to other micro-organisms, but we can apply a different primitive boundary condition for the squirmers to see whether the effect of this are significant. In this boundary condition, the surface squirming velocity is defined as $\lambda \boldsymbol{u}_s$. Here $\boldsymbol{u}_s$ is the normal squirming velocity defined by (A 8) and λ is a scalar factor that is chosen to realize constant swimming power, equal to the rate of viscous-energy dissipation, throughout an interaction. The swimming power consumed by a squirmer is defined as

$$\int_A \boldsymbol{\tau} \cdot \boldsymbol{u}_s \, \mathrm{d}A, \tag{6.1}$$

where $\boldsymbol{\tau}$ is the traction force on the surface. The factor λ can be calculated easily by exploiting the linearity of the flow field. The flow field generated by two squirmers is the sum of the flow fields in the following two cases (i) sphere 1 has the squirming motion and sphere 2 is inert; (ii) sphere 1 is inert and sphere 2 has the squirming motion. In the case of an inert sphere the swimming power is zero. Therefore λ can be determined separately for a sphere with squirming motion in each flow field.

We have checked the relative translational–rotational velocities under the constant-swimming-power condition. In fact the effect of changing the boundary condition was very small. This can be explained as follows. The surface velocity is proportional to λ, and the lubrication force, (3.39), is proportional to $\log \varepsilon^{-1}$ and λ. The power is the product of these two quantities in the near field and is thus proportional to $\log \varepsilon^{-1}$ and λ^2. In order to keep the power constant, λ should therefore vary as

$$\lambda \propto \sqrt{\frac{1}{\log \varepsilon^{-1}}}. \tag{6.2}$$

Because $\log \varepsilon^{-1}$ is a very weak singularity, λ changes very slowly.

In future papers, we will use the database compiled in this paper to investigate both the rheological properties of a semi-dilute suspension of many squirmers and also the diffusive property of squirmers in a semi-dilute suspension (Ishikawa & Pedley 2006*a*, *b*).

T. Ishikawa was supported by a JSPS postdoctoral fellowship for research abroad from 2003 to 2005. M. P. Simmonds was supported by a NERC research studentship from 1999 to 2002.

Appendix A. Solutions in dyadic notation for a solitary squirmer

The aim of this appendix is to establish the solutions for the flow and the stresslet generated by a single squirmer, and to represent them in dyadic notation. This provides frame-independent expressions, which will be used throughout the paper. The initial part of this derivation is taken directly from Blake (1971). In this appendix it is irrelevant whether the squirmer is bottom heavy or not.

Solving the Stokes equations for an axisymmetric nearly spherical body with a prescribed (and not necessarily zero) velocity on its surface, in an otherwise static fluid, reduces to solving

$$\mu \nabla^2 \boldsymbol{u} = \nabla p, \qquad \nabla \cdot \boldsymbol{u} = 0, \tag{A 1}$$

where the velocity of the fluid is $\boldsymbol{u}$, its viscosity is μ and p is the pressure. In a frame of reference in which the sphere centre is at rest, and the fluid at infinity has velocity $-U\boldsymbol{e}$ (where $\boldsymbol{e}$ is the unit vector along the axis of symmetry and U is the speed at

which the sphere swims), the following boundary conditions are then applied for a sphere to be termed a *squirmer*:

$$u_r|_{r=a} = \sum_n A_n(t) P_n(\cos\theta), \qquad u_\theta|_{r=a} = \sum_n B_n(t) V_n(\cos\theta), \tag{A 2}$$

where P_n is the nth Legendre polynomial and V_n is defined thus:

$$V_n(\cos\theta) = \frac{2}{n(n+1)} \sin\theta \, P_n'(\cos\theta); \tag{A 3}$$

u_r and u_θ are the velocities in the r- and θ-directions (using spherical polar coordinates). The spherical coordinates are defined such that $\theta = 0$ denotes the axis of axisymmetry and thus the swimming direction. This problem can be solved and the solution (Blake 1971) is:

$$\begin{aligned} u_r = &-U\cos\theta + A_0\frac{a^2}{r^2}P_0 + \frac{2}{3}(A_1+B_1)\frac{a^3}{r^3}P_1 \\ &+ \sum_{n=2}^{\infty}\left[\left(\frac{n}{2}\frac{a^n}{r^n} - \left(\frac{n}{2}-1\right)\frac{a^{n+2}}{r^{n+2}}\right)A_nP_n + \left(\frac{a^{n+2}}{r^{n+2}} - \frac{a^n}{r^n}\right)B_nP_n\right], \end{aligned} \tag{A 4}$$

$$\begin{aligned} u_\theta = &\, U\sin\theta + \frac{1}{3}(A_1+B_1)\frac{a^3}{r^3}V_1 \\ &+ \sum_{n=2}^{\infty}\left[\left(\frac{n}{2}\frac{a^{n+2}}{r^{n+2}} - \left(\frac{n}{2}-1\right)\frac{a^n}{r^n}\right)B_nV_n + \frac{n}{2}\left(\frac{n}{2}-1\right)\left(\frac{a^n}{r^n} - \frac{a^{n+2}}{r^{n+2}}\right)A_nV_n\right], \end{aligned} \tag{A 5}$$

$$p = \mu\sum_{n=2}^{\infty}\frac{2n-1}{n+1}(nA_n - 2B_n)\frac{a^n}{r^{n+1}}P_n. \tag{A 6}$$

For the squirmer to experience no net force (a necessity since it is neutrally buoyant and the Reynolds number is zero),

$$U = \frac{1}{3}(2B_1 - A_1). \tag{A 7}$$

In the case of zero radial velocity on the sphere surface ($A_n = 0\,\forall n$), the only case considered in this paper, the expression for the velocity can be written in a form independent of basis. Transforming now to a frame of reference in which the fluid at infinity is at rest, one can express the velocity field (A 4), (A 5) in terms of $\boldsymbol{e}$, $\boldsymbol{r}$ and r, where $\boldsymbol{e}$ is the swimming direction or orientation vector of a squirmer, $\boldsymbol{r}$ is the position vector and $r = |\boldsymbol{r}|$, as follows:

$$\begin{aligned} \boldsymbol{u} = &-\frac{1}{3}\frac{a^3}{r^3}B_1\,\boldsymbol{e} + B_1\frac{a^3}{r^3}\frac{\boldsymbol{e}\cdot\boldsymbol{r}}{r}\frac{\boldsymbol{r}}{r} + \sum_{n=2}^{\infty}\left(\frac{a^{n+2}}{r^{n+2}} - \frac{a^n}{r^n}\right)B_nP_n\left(\frac{\boldsymbol{e}\cdot\boldsymbol{r}}{r}\right)\frac{\boldsymbol{r}}{r} \\ &+ \sum_{n=2}^{\infty}\left(\frac{n}{2}\frac{a^{n+2}}{r^{n+2}} - \left(\frac{n}{2}-1\right)\frac{a^n}{r^n}\right)B_nW_n\left(\frac{\boldsymbol{e}\cdot\boldsymbol{r}}{r}\right)\left(\frac{\boldsymbol{e}\cdot\boldsymbol{r}}{r}\frac{\boldsymbol{r}}{r} - \boldsymbol{e}\right). \end{aligned} \tag{A 8}$$

Here W_n is defined by

$$W_n(\cos\theta) = \frac{2}{n(n+1)}P_n'(\cos\theta). \tag{A 9}$$

The expression for the velocity is now independent of the coordinate frame.

The stresslet generated by a solitary squirmer can now be calculated. The problem is linear in velocity (since the Reynolds number is zero) so the stresslet can be calculated for each individual mode of squirming, where a *mode* refers to the motion driven by only one of the B_n. Consider the terms that have a factor B_n (i.e. set $B_i = 0 \,\forall\, i \neq n$). The velocity field is given by

$$\boldsymbol{u} = \frac{a^n}{r^n} B_n \left[\left(\frac{a^2}{r^2} - 1 \right) P_n \frac{\boldsymbol{r}}{r} + \left(\frac{a^2}{r^2} \frac{n}{2} - \left(\frac{n}{2} - 1 \right) \right) \left(\frac{\boldsymbol{e}\cdot\boldsymbol{r}}{r} \frac{\boldsymbol{r}}{r} - \boldsymbol{e} \right) W_n \right] \tag{A 10}$$

for $n \neq 1$. P_n and W_n must be considered as functions of $\boldsymbol{e}\cdot\boldsymbol{r}/r$. The rate of strain $\mathscr{E}$, say, can then be calculated on the sphere (where $r = a$):

$$\begin{aligned} \mathscr{E} = \frac{B_n}{2a} \Big[& -4 P_n \frac{\boldsymbol{r}\boldsymbol{r}}{a^2} - 4(n+1) \frac{\boldsymbol{e}\cdot\boldsymbol{r}}{a} \frac{\boldsymbol{r}\boldsymbol{r}}{a^2} W_n + (2n+1)(\boldsymbol{e}\boldsymbol{r} + \boldsymbol{r}\boldsymbol{e}) W_n \\ & + 2 \frac{\boldsymbol{e}\cdot\boldsymbol{r}}{a} W_n \boldsymbol{I} + 2 \left(\frac{\boldsymbol{e}\cdot\boldsymbol{r}}{a} \frac{\boldsymbol{r}\boldsymbol{e} + \boldsymbol{e}\boldsymbol{r}}{a} - \frac{\boldsymbol{r}\boldsymbol{r}}{a^2} - \boldsymbol{e}\boldsymbol{e} \right) W_n' \Big] . \end{aligned} \tag{A 11}$$

The stresslet $\boldsymbol{S}$ was defined by Batchelor & Green (1972*b*) to give no isotropic contribution, and is given by

$$\boldsymbol{S} = \int_A \left[\tfrac{1}{2} ((\boldsymbol{\sigma}\cdot\boldsymbol{n})\boldsymbol{x} + \boldsymbol{x}(\boldsymbol{\sigma}\cdot\boldsymbol{n})) - \tfrac{1}{3} \boldsymbol{x}\cdot\boldsymbol{\sigma}\cdot\boldsymbol{n}\boldsymbol{I} - \mu (\boldsymbol{u}\boldsymbol{n} + \boldsymbol{n}\boldsymbol{u}) \right] \mathrm{d}A, \tag{A 12}$$

where $\boldsymbol{\sigma}$ is the stress tensor,

$$\boldsymbol{\sigma} = -p\boldsymbol{I} + 2\mu\mathscr{E}, \tag{A 13}$$

and the particle surface is defined as A. In the case of a squirmer, the last term in the integral does not vanish. All terms in (A 12) integrate to zero when n is odd. When n is even and $n \neq 2$ the terms are not identically zero, but sum to zero. In the case where $n = 2$ the result is non-zero and is

$$\boldsymbol{S} = \frac{4}{3} \pi \mu a^2 (3\boldsymbol{e}\boldsymbol{e} - \boldsymbol{I}) B_2. \tag{A 14}$$

The benefit of the initial decomposition of the velocity field on the squirmer is now clear. The first mode determines the swimming speed (A 7) and the second mode determines the stresslet of the squirmer (A 14). The squirming parameter β is defined as B_2/B_1. In all the examples calculated explicitly in this paper we chose $B_n = 0$ for $n > 2$.

Appendix B. Stresslet expressed by the single-layer potential

When the Reynolds number is zero, a flow field external to a squirmer can be given in integral form, using a single-layer potential only, as (4.1). The boundary-element method using single- or double-layer potentials only, so called the generalized boundary-integral method, is explained in detail, with a derivation of the integral equations and of the force and torque exerted on a particle, in an established text (Pozrikidis 1992).

The single-layer potential $\boldsymbol{q}$, (4.2), is found by subtracking the traction force on the inner surface, $\boldsymbol{f}_{in}$, from that on the outer surface, $\boldsymbol{f}_{out}$. Equation (4.1) with the boundary condition (4.3) expresses the velocity field generated by point forces in a homogeneous fluid and is not restricted to a rigid-body motion inside a squirmer. In order to impose a rigid-body motion, one needs to introduce a double-layer potential in (4.1) and to deal with velocity slip on the surface explicitly. Introducing double-layer potentials, however, considerably increases the computational load. Since the

effect of $\boldsymbol{f}_{in}$ appears in calculating the stresslet of a squirmer, we intend to subtract its effect analytically in the following manner.

The first moment of the single-layer potential can be expressed as

$$\int_A \boldsymbol{xq}\,\mathrm{d}A = \int_{A_{out}} \boldsymbol{x}\boldsymbol{f}_{out}\,\mathrm{d}A - \int_{A_{in}} \boldsymbol{x}\boldsymbol{f}_{in}\,\mathrm{d}A, \tag{B 1}$$

where A_{out} and A_{in} represent the outer and inner surfaces, respectively. The second integral can be transformed, by exploiting the discussion in Batchelor (1970) and equation (A 13), as follows:

$$\begin{aligned}\int_{A_{in}} \boldsymbol{x}\boldsymbol{f}_{in}\,\mathrm{d}A &= \int_{A_{in}} \boldsymbol{x}(\boldsymbol{\sigma}\cdot\boldsymbol{n})\,\mathrm{d}A = \int_{V_{in}} \boldsymbol{\sigma}\,\mathrm{d}V + \int_{V_{in}} \boldsymbol{x}(\nabla\cdot\boldsymbol{\sigma})\,\mathrm{d}V \\ &= \int_{V_{in}} (-p\boldsymbol{I} + 2\mu\mathscr{E})\,\mathrm{d}V = IT + \mu\int_{A_{in}} (\boldsymbol{un} + \boldsymbol{nu})\,\mathrm{d}A \end{aligned} \tag{B 2}$$

where V_{in} is the volume inside the A_{in}, and IT is the isotropic contribution term. The flow field expressed by (4.1) has no slip velocity on the surface, so the last integral in (B 2) can be substituted to the outer surface from the inner surface. Thus equation (B 1) can be rewritten as

$$\int_A \boldsymbol{xq}\,\mathrm{d}A = \int_{A_{out}} \boldsymbol{x}\boldsymbol{f}_{out}\,\mathrm{d}A - \mu\int_{A_{out}} (\boldsymbol{un} + \boldsymbol{nu})\,\mathrm{d}A. \tag{B 3}$$

This equation is exactly the same as the stresslet given by Batchelor (1970), in which the isotropic contribution and asymmetric part have not yet been subtracted. Consequently, the stresslet of squirmer m can be expressed using only a single-layer potential:

$$\boldsymbol{S}_m = \int_{A_m} \left[\tfrac{1}{2}(\boldsymbol{qx} + \boldsymbol{xq}) - \tfrac{1}{3}\boldsymbol{x}\cdot\boldsymbol{q}\boldsymbol{I}\right]\mathrm{d}A. \tag{B 4}$$

REFERENCES

Batchelor, G. K. 1970 The stress system in a suspension of force-free particles. *J. Fluid Mech.* **41**, 545–570.

Batchelor, G. K. & Green, J. T. 1972*a* The hydrodynamic interaction of two small freely-moving spheres in a linear flow field. *J. Fluid Mech.* **56**, 375–400.

Batchelor, G. K. & Green, J. T. 1972*b* The determination of the bulk stress in a suspension of spherical particles to order c^2. *J. Fluid Mech.* **56**, 401–427.

Baygents, J. C., Rivette, N. J. & Stone, H. A. 1998 Electrohydrodynamic deformation and interaction of drop pairs. *J. Fluid Mech.* **368**, 359–375.

Bees, M. A. & Hill, N. A. 1998 Linear bioconvection in a suspension of randomly-swimming, gyrotactic micro-organisms. *Phys. Fluids* **10**, 1864–1881.

Blake, J. R. 1971 A spherical envelope approach to ciliary propulsion. *J. Fluid Mech.* **46**, 199–208.

Brady, J. F. & Bossis, G. 1988 Stokesian dynamics. *Annu. Rev. Fluid Mech.* **20**, 111–157.

Brennen, C. 1974 An oscillating-boundary-layer theory for ciliary propulsion. *J. Fluid Mech.* **65**, 799–824.

Brennen, C. & Winet, H. 1977 Fluid mechanics of propulsion by cilia and flagella. *Annu. Rev. Fluid Mech.* **9**, 339–398.

Childress, S., Levandowsky, M. & Spiegel, E. A. 1975 Pattern formation in a suspension of swimming micro-organisms: equations and stability theory. *J. Fluid Mech.* **63**, 591–613.

Claeys, I. L. & Brady, J. F. 1989 Lubrication singularities of the grand resistance tensor for two arbitrary particles. *PhysicoChemi. Hydrodyn.* **11**, 261–293.

Claeys, I. L. & Brady, J. F. 1993 Suspensions of prolate spheroids in Stokes flow. Part 1. Dynamics of a finite number of particles in an unbounded fluid. *J. Fluid Mech.* **251**, 411–442.

Durlofsky, L., Brady, J. F. & Bossis, G. 1987 Dynamic simulation of hydrodynamically interacting particles. *J. Fluid Mech.* **180**, 21–49.

Fasham, M. J. R., Ducklow, H. W. & McKelvie, S. M. 1990 A nitrogen-based model of plankton dynamics in the oceanic mixed layer. *J. Mar. Res.* **48**, 591–639.

Goldman, A. J., Cox, R. G. & Brenner, H. 1966 The slow motion of two identical arbitrarily oriented spheres through a viscous fluid. *Chem. Engng Sci.* **21**, 1151–1170.

Guell, D. C., Brenner, H., Frankel, R. B. & Hartman, H. 1988 Hydrodynamic forces and band formation in swimming magnetotactic bacteria. *J. Theor. Biol.* **135**, 525–542.

Hill, N. A. & Häder, D.-P. 1997 A biased random walk model for the trajectories of swimming micro-organisms. *J. Theor. Biol.* **186**, 503–526.

Hillesdon, A. J., Pedley, T. J. & Kessler, J. O. 1995 The development of concentration gradients in a suspension of chemotactic bacteria. *Bull. Math. Biol.* **57**, 299–344.

Ingber, M. S. & Mammoli, A. A. 1999 A comparison of integral formulations for the analysis of low Reynolds number flow. *Engng Anal. Bound. Elem.* **23**, 307–315.

Ishikawa, T. & Pedley, T. J. 2006*a* The rheology of a semi-dilute suspension of swimming model micro-organisms. *J. Fluid Mech.* (submitted).

Ishikawa, T. & Pedley, T. J. 2006*b* Diffusion of swimming model micro-organisms in a semi-dilute suspension. *J. Fluid Mech.* (submitted).

Jiang, H., Osborn, T. R. & Meneveau, C. 2002 Hydrodynamic interaction between two copepods: a numerical study. *J. Plank. Res.* **24**, 235–253.

Ken, H. J. & Anderson, J. L. 1985 Boundary effects on electrophoretic motion of colloidal spheres. *J. Fluid Mech.* **153**, 417–439.

Kessler, J. O. 1986 The external dynamics of swimming micro-organisms. In *Progress in Phycological Research* (ed. F. E. Round & D. J. Chapman), Vol. 4, pp. 257–307. Bristol: Biopress.

Kessler, J. O., Hoelzer, M. A., Pedley, T. J. & Hill, N. A. 1994 Functional pattern of swimming bacteria In *Mechanics and Physiology of Animal Swimming* (ed. L. Maddock, Q. Bone & J. M. V. Rayner), pp. 3–12. Cambridge University Press.

Kim, S. & Karrila, S. J. 1992 *Microhydrodynamics: Principles and Selected Applications.* Butterworth Heinemann.

Larson, A., Kirk, M. M. & Kirk, D. L. 1992 Molecular phylogeny of the Volvocine flagellates. *Mol. Biol. Evol.* **9**, 85–105.

Lega, J. & Passot, T. 2003 Hydrodynamics of bacterial colonies. *Phys. Rev.* E**67**, 1906.

Lighthill, M. J. 1952 On the squirming motion of nearly spherical deformable bodies through liquids at very small Reynolds numbers. *Comm. Pure Appl. Math.* **5**, 109–118.

Lyness, J. N. & Jespersen, D. 1975 Moderate degree symmetric quadrature rules for the triangle. *J. Inst. Maths Applics.* **15**, 19–32.

Magar, V., Goto, T. & Pedley, T. J. 2003 Nutrient uptake by a self-propelled steady squirmer. *Q. J. Mech. Appl. Maths* **56**, 65–91.

Metcalfe, A. M. & Pedley, T. J. 2001 Falling plumes in bacterial bioconvection. *J. Fluid Mech.* **445**, 121–149.

Metcalfe, A. M., Pedley, T. J. & Thingstad, T. F. 2004 Incorporating turbulence into a plankton foodweb model. *J. Mar. System* **49**, 105–122.

Nasseri, S. & Phan-Thien, N. 1997 Hydrodynamic interaction between two nearby swimming micromachines. *Comput. Mech.* **20**, 551–559.

Nott, P. R. & Brady, J. F. 1994 Pressure-driven flow of suspensions: simulation and theory. *J. Fluid Mech.* **275**, 157–199.

O'Neill, M. E. & Stewartson, K. 1967 On the slow motion of a sphere parallel to a nearby plane wall. *J. Fluid Mech.* **27**, 705–724.

Pedley, T. J. & Kessler, J. O. 1987 The orientation of spheroidal microorganisms swimming in a flow field. *Proc. R. Soc. Lond.* B **231**, 47–70.

Pedley, T. J. & Kessler, J. O. 1990 A new continuum model for suspensions of gyrotactic micro-organisms. *J. Fluid Mech.* **212**, 155–182.

Pedley, T. J. & Kessler, J. O. 1992 Hydrodynamic phenomena in suspensions of swimming microorganisms. *Annu. Rev. Fluid Mech.* **24**, 313–358.

Pitta, T. P. & Berg, H. C. 1995 Self-electrophoresis is not the mechanism for motility in swimming cynobacteria. *J. Bacteriology* **177**, 5701–5703.

Pozrikidis, C. 1992 *Boundary Integral and Singularity Methods for Linearized Viscous Flow*, chapter 4. Cambridge University Press.

Prieve, D. C., Anderson, J. L., Ebel, J. P. & Lowell, M. E. 1984 Motion of a particle generated by chemical gradients. Part 2. Electrolytes. *J. Fluid Mech.* **148**, 247–269.

Ramia, M., Tullock, D. L. & Phan-Thien, N. 1993 The role of hydrodynamic interaction in the locomotion of microorganisms. *Biophysical J.* **65**, 755–778.

Russel, W. B., Saville, D. A. & Schowalter, W. R. 1992 *Colloidal Dispersions.* Cambridge University Press.

Stone, H. A. & Samuel, A. D. T. 1996 Propulsion of microorganisms by surface distortions. *Phys. Rev. Lett.* A **77**, 4102–4104.

Tran-Cong, T. & Phan-Thien, N. 1989 Stokes problems of multiparticle systems: a numerical method for arbitrary flows. *Phys. Fluids* A **1**, 453–461.

Vladimirov, V. A., Wu, M. S. C., Pedley, T. J. *et al.* 2004 Measurement of cell velocity distributions in populations of motile algae. *J. Expl Biol.* **207**, 1203–1216.

Waterbury, J. B., Willey, J. M., Franks, D. G. *et al.* 1985 A cyanobacterium capable of swimming motility. *Science* **230**, 74–76.

Youngren, G. K. & Acrivos, A. 1975 Stokes flow past a particle of arbitrary shape: a numerical method of solution. *J. Fluid Mech.* **69**, 377–403.